Modeling of chemical vapor infiltration processes

17

G.L. Vignoles
University of Bordeaux, Pessac, France

17.1 Introduction

As described in Chapter 12, the chemical vapor infiltration process is among the most interesting processes for the preparation of ceramic–matrix composites (CMCs). However, its overall cost, its optimization, and sometimes even its control are important issues. This is why process modeling is of interest. It can help in finding the best directions to improve the process efficiency while preserving or even improving the material quality, at a lower cost than carrying out systematic experimental explorations of the processing parameter space.

Modeling can span a whole range of accuracy and, simultaneously, of computational expense. Very detailed numerical models are able to give precise insights in a given test case but are very difficult to run over and over by varying the processing conditions; on the other hand, lightweight analytic or quasi-analytic models, though less realistic, are suited to follow the influence of the process parameters.

CVI modeling raises a certain number of difficulties. First, chemical reactions and transfer phenomena are intimately coupled; second, the presence of an evolutive porous medium implies the necessity of handling several space scales. So, it is a multiscale, multiphysics modeling task that is required for this case.

In this chapter, we will address a survey of CVI modeling. First, the basic ingredients of the models will be recalled and briefly discussed. The next part will review some numerical techniques and modeling strategies. Then, two examples of CVI modeling approaches will be presented, concerning carbon/carbon and CMCs. Variations other than isobaric, isothermal CVI will be addressed in the next part. Finally, some conclusive remarks will be given.

17.2 Process analysis and modeling strategy

The CVI process (Naslain and Langlais, 1986; Naslain et al., 2006) is based on the interactions between transport of chemical species and their reaction, inside and outside of the porous medium constituted by the fibrous preform. Externally, it resembles the CVD process (Pierson, 1988); however, seen from the porous medium, it looks more like a problem of progressive plugging of a filter or to the deactivation of a catalyst by some parasitic reaction. The following phenomena, therefore, have to be accounted for:

1. *Heat transfer to the solids*. Depending on the variation of CVI, many situations may occur. The fibrous preforms may be placed inside a hot-wall apparatus and thus receive heat by

Advances in Composites Manufacturing and Process Design. http://dx.doi.org/10.1016/B978-1-78242-307-2.00017-8

radiation and conduction, or be heated by induction or even by resistive heating. In the latter cases, creation of heat by the Joule effect has to be accounted for—and this may lead to a full solution of electromagnetic or electrokinetic problems.

2. *Heat transfer to the gases*. As opposed to solids, the gases lying outside the preform are difficult to bring to the desired cracking and deposition temperature; accordingly, as far as they are concerned, heat transfer is intimately linked to mass transfer. On the other hand, as soon as these gases enter the porous medium, their exchange surface being very high, they reach the solid phase temperature very quickly.
3. *Gas convection in the infiltration chamber*. The most common conditions used in I-CVI are such that the gas flow pattern is laminar. However, this is not necessarily always the case, and recirculations due to natural convection or something else may occur.
4. *Gas diffusion in the infiltration chamber*. This includes multicomponent diffusion in laminar flow conditions, and possibly thermodiffusion (Soret effect) in the case of severe thermal gradients.
5. *Gas transport in the porous medium, featuring multicomponent diffusion, viscous transport, and Knudsen (rarefied) diffusion*. Here, the equivalent of the Soret effect is called thermal transpiration.
6. *Homogeneous gas reactions in the deposition chamber and inside the porosity of the preform*. Some reactions involving unimolecular steps are pressure dependent.
7. *Heterogeneous (gas–solid) reactions at reactor walls and at the internal surface of the preform*.
8. *Porous medium structural evolution*. It has an influence on heat transfer properties, on internal gas flow, and on the effective reaction rates—less volume for homogeneous reactions and more surface for the heterogeneous ones.

These phenomena are summarized in Figure 17.1, except the porous medium structural evolution, which is in most cases much slower than the preceding ones.

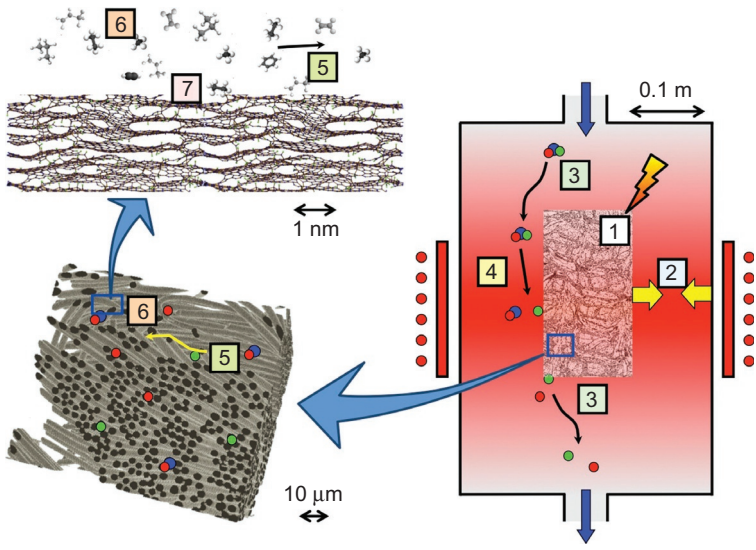

Figure 17.1 Scales and phenomena in a CVI reactor. Right: reactor scale; lower left: preform (fibrous medium) scale; upper left: nanometer scale.

Accordingly, a usual assumption is to treat all gas-related phenomena (transport and reactions) as in a quasi-steady state; the porous medium properties may be updated from the knowledge of this quasi-steady state.

Several scales are recognized in this description:

- A macroscopic scale, concerning the whole reactor plus the preforms inserted in it, considered as homogeneous.
- A mesoscopic scale, related to the structural and textural details of the preform. The fiber diameter is of the order of a few micrometers, but larger scales related to weavings, stackings, etc., may be present.
- A microscopic scale, at which the chemical phenomena take place.

It appears from this description that the deposition rate at a given location in the porous medium occurs as the result of several phenomena chained in series. To yield a solid, the precursor gas has to be first brought by convection/diffusion (in parallel with each other) to the porous medium, then inside it, possibly undergo some chemical evolution before reaching the surface, and finally react with the latter. As a consequence, the slowest of these phenomena will be the governing one.

Inside the porous medium, the transfer phenomena are somewhat intricate. Indeed, the rarefied gas transfer contributes both to diffusion and convection, making it difficult to separate the treatment of fluxes, as illustrated in Figure 17.2. Moreover, evaluation of transfer inside these porous media requires some kind of averaging procedure, as will be seen later.

A global scheme is proposed in Figure 17.3: the idea is to sum-up all knowledge inside a possibly unique modeling tool that can be used for predictions and process optimization. Three important parts are required. The first is a reactor-scale solver that integrates information from lower scales: on one hand, transport in evolutive porous

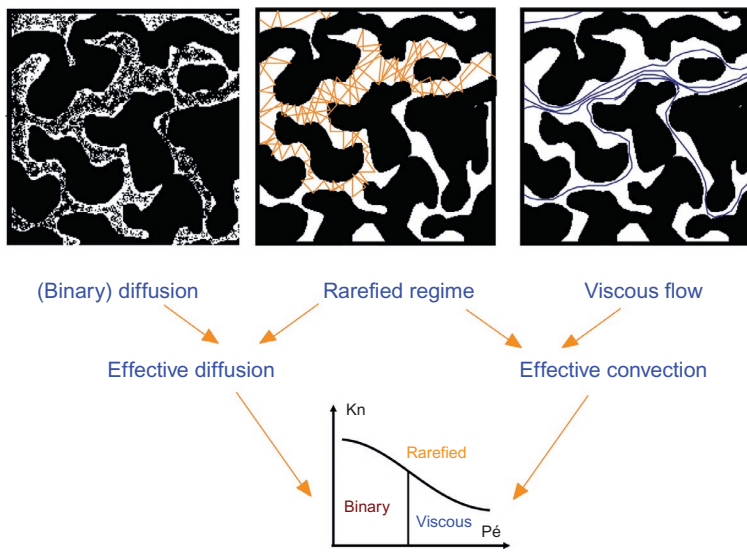

Figure 17.2 Different transfer modes in a porous medium.

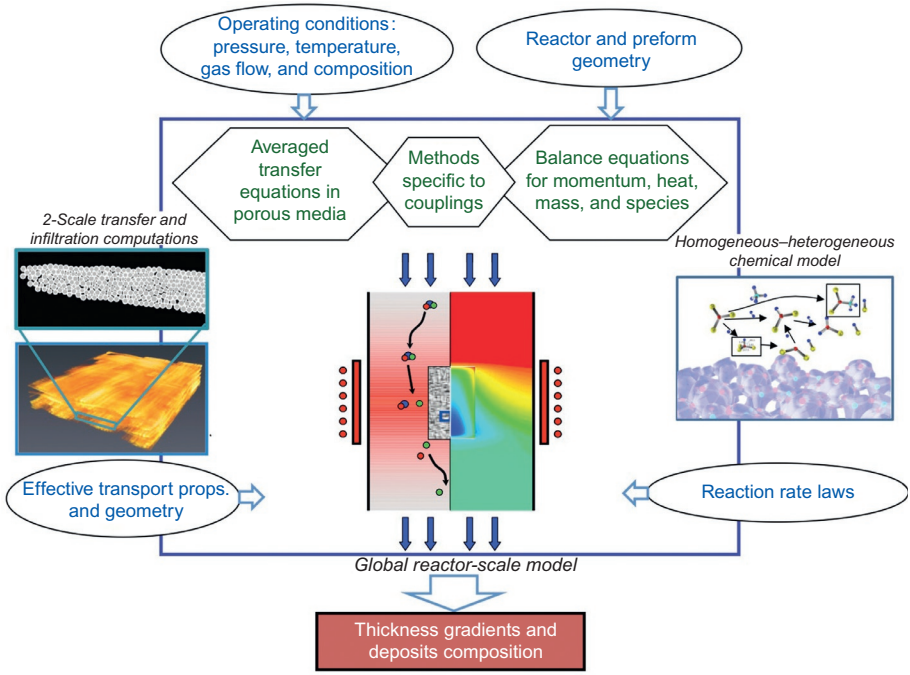

Figure 17.3 Global strategy for CVI modeling.

media, and on the other hand, chemical reaction rates. In the following sections, we will address these points in more detail.

17.3 Analytical and simplified models

Large-mesh simulations with detailed physics are a powerful tool for process scale-up and control; however, many works have focused on 1-D simulations restricted to the preform (see Table 17.1), which is numerically much lighter and manages to provide useful information; with further simplifications on the physics and chemistry, analytical estimates for infiltration time and quality have been produced (Langlais, 2000). Many early models reduced the description of the porous medium to a single pore; there was only one diffusing species, only one deposition reaction with first-order kinetics, no homogeneous reactions, no temperature gradients, no detailed coupling with the surrounding gas, no evolution of the porous medium structure, and so on. Either purely analytical relations were derived, or simple numerical integrations over a 1-D or 2-D, 1-variable equation on the reactant concentration $C = P_g/\mathcal{R}T$, reading as:

$$\frac{\partial}{\partial z}\left(-r_p^2 D_g \frac{\partial C}{\partial z}\right) = -2 r_p k_{\text{het}} C \tag{17.1}$$

In addition, the time evolution of the radius is given by

$$\frac{\mathrm{d}}{\mathrm{d}t}r_p = -rk_{\mathrm{het}}C\frac{M_s}{\rho_s} \tag{17.2}$$

Carolan and Michaels (1987) have developed a single-pore model following these hypotheses and have predicted, in the case of zirconia deposition from $ZrCl_4/H_2O$, the time to pore plugging and the deposition profile. They showed that they were only depending on a single Thiele modulus (Thiele, 1939)

$$\Phi = L\sqrt{\frac{k_{\mathrm{het}}\sigma_v}{\varepsilon D_g}} \tag{17.3}$$

where $\sigma_v/\varepsilon = 2/r$. When the Thiele modulus becomes comparable to 1 or higher, then diffusional limitations will prevent the process from achieving a homogeneous enough infiltration; this can be overcome by lowering temperature or pressure, but at the expense of increasing the total infiltration time (Xu and Yan, 2012). Indeed, a characteristic infiltration time is:

$$\tau = \frac{\rho_s \mathcal{R}T}{M_s P_g \sigma_v k_{\mathrm{het}}} \tag{17.4}$$

Following early attempts by van den Brekel et al. (1981) and Rossignol et al. (1984), Tai and Chou (1988, 1989) have studied the effect of temperature on the infiltration of a single pore by alumina or titanium carbide. They have found that increasing temperature would be harmful to the deposit homogeneity by accelerating the gas deposition kinetics with respect to the diffusion rate. The influence was summarized in a Sherwood (or Damköhler) number $Sh = k_{\mathrm{het}}r_p/D_g$, which is very closely related to the Thiele modulus. No clear solution of the infiltration equation (i.e., here, the radius time decrease equation) was provided, as pointed out by Currier and Valone (1990). Fitzer et al. (1992) have extended this study to predict SiC deposit thicknesses and checked the validity of their results with respect to experimental data. Fédou et al. (1993) has carried out a numerical solution in the case of SiC deposition and validated with respect to actual single-pore experiments. Tsai and Desu (1991) have validated a similar model on the same data; adding the contribution of forced flow showed a poor influence at high temperatures. Grujicic (1994) has studied the deposition of TiB_2 and shown the influence of the Knudsen number, showing that neglecting Knudsen transport in typical CVI conditions enhances strongly the gas flux and accelerates the deposition, as compared to a model neglecting Knudsen diffusion. Griffiths and Nilson (1998) employed a combined analytical and numerical method to optimize process conditions for I-CVI of boron nitride. An optimum pressure yielding the maximum deposition rate at a preform center is obtained in closed form and is found to depend only on the activation energy of the deposition reaction, the characteristic pore size, and properties of the reactant and product gases. Optimum temperatures are obtained using an analytical expression for the optimum value along with numerical solutions to the governing transport equations.

Lu (1993) considered a random pore model instead of a single-pore model, and his conclusions were similar to the single-pore ones. Yoshikawa and Evans (2002)

modified the simple reaction-diffusion equation in a single pore by changing the pore shape; optimal fictitious pore shapes were thus obtained.

Contrary to most single-pore studies focused on the initial deposition rate profile, and following an initial optimization study of Chang et al. (1997, 1998) and Ditkowski et al. (2000), then Jones (2006, 2007) have managed to produce asymptotic estimates of the infiltration profile up to the end of the process in the case of small Thiele modulus, allowing the distinction of successful and unsuccessful infiltrations (i.e., where porosity gradients are less or more than a given threshold). Numerical results confirm the analytical estimates. Optimized temperature and pressure programs during infiltration are suggested.

Still, on the basis of single-pore models, the effect of chemical rate laws has been investigated. Nonlinear chemical kinetics may be useful in helping to achieve uniform density, as shown by Middleman in a theoretical single-pore model (Middleman, 1989), then by Xomeritakis and Lin in the case of zirconia deposition inside membranes with quasi-zero order kinetics (Xomeritakis and Lin, 1994). Zhang et al. have designed a multistep kinetic model for the deposition of pyrolytic carbon from hydrocarbons. Inside-out isothermal infiltration is proved to be possible on the basis of these nonlinear kinetic schemes. Dekker et al. (1996), working on CVI of TiN, TiB_2, and TiC, have considered several deposition kinetic laws, including or not adsorbed intermediates, in order to compare the deposition profiles to experimental data. Chang et al. (1997) have also tested various partial orders of the deposition rate law with respect to the precursor and have shown that the choice of the model had an appreciable influence on the deposited profiles and on the optimal infiltration pressure.

Reuge and Vignoles (2005) have proposed a simple model to account for the interaction between the porous medium and its surrounding fluid. As could be expected, two dimensionless numbers arise from this case study: a reaction/diffusion ratio, similar to a Damköhler number, and a convection/diffusion ratio. The initial reactant depletions in the cavity before reaching the porous sample and inside it were obtained analytically as a function of these two numbers, evidencing an optimal zone in parameter space.

All the single-pore models presented above have the great benefit of giving hints on the influence of operating conditions on the process efficiency, but they have their limits in terms of accuracy. Indeed, the fibrous preforms used in industry are very complex porous media that a single pore could not represent efficiently. Other phenomena such as temperature/pressure gradients, coupling with the surrounding fluid, and so on were poorly accounted for. Therefore, many modeling approaches paying attention to these porous media have been developed, as described in the next sections.

17.4 Reactor-scale models

As opposed to the early models described above, a full model has to provide a more detailed description of the phenomena taking place. In this section, the necessary balance equations will be reviewed, before discussing the numerical methods.

Table 17.1 Comparative presentation of single-pore models for I-CVI

References	Transport	Chemical system	Comments
Carolan and Michaels (1987)	Knudsen diff.	ZrO_2 from $ZrCl_4/H_2O$	Runge-Kutta fourth order
Rossignol et al. (1984)	Plain diffusion	TiC from $TiCl_4/CH_4$	
Tai and Chou (1988, 1989)	Knudsen and binary diff.	Al_2O_3 from $CO_2/H_2/AlCl_3$ and TiC from $TiCl_4/CH_4$	Analytical, simplified evolution of pore radius
Fitzer et al. (1992)	Plain diffusion	SiC from CH_3SiCl_3	Analytical, simplified pore radius evolution
Fédou et al. (1993)	Knudsen and binary diff.	SiC from CH_3SiCl_3	Finite differences
Tsai and Desu (1991)	Added forced flow	SiC from CH_3SiCl_3	Finite differences
Grujicic (1994)	Knudsen and binary diff.	TiB_2 from $TiCl_4/BCl_3/H_2$	Influence of Kn number
Griffiths and Nilson (1998)	Knudsen and binary diff.	BN from $BCl_3/NH_3/H_2$	Optimization of processing conditions
Zhang and Hüttinger (2001, 2002)	id.	C from C_nH_m/H_2	Initial profiles only; multistep chemistry
Lu (1993)	id.	Any, first order	Random pore model similar to single-pore
Yoshikawa and Evans (2002)	id.	Any, first order	"Most infiltrable pore" by varying initial pore profile
Chang et al. (1997), Ditkowski et al. (2000)	id.	Any, first order	Optimization of parameter programs
Jones (2006, 2007)	Knudsen diff.	C from CH_4/H_2	Optimization of parameter programs
Chang et al. (1998)		Any, first order	Effect of nonlinear kinetics
Middleman (1989)	Plain diffusion	$A \rightarrow B \rightarrow$ deposit	Inverse profile
Xomeritakis and Lin (1994)	Knudsen and binary diff.	ZrO_2 from $ZrCl_4/H_2O$	Quasi-zero order kinetics
Dekker et al. (1996)	id.	TiN, TiB_2, TiC from $TiCl_4$	Influence of kinetic schemes
Minkina (1997)	Coupling with surrounding fluid	Si_3N_4 from $(CH_3)_6Si_2/NH_3$	
Reuge and Vignoles (2005)	Coupling with surrounding fluid	SiC from CH_3SiCl_3/H_2	Analytical at initial time

17.4.1 Balance equations

Reactor-scale models are based on several balance equations, as described below. As the main purpose of CVI is to deposit a solid inside a preform, the first equation to be accounted for is the deposition equation. It is a *solid mass balance equation* and relates the solid growth rate to the precursor gas net incoming flow rate. *Species mass balance equations* may, therefore, be solved for each gas species. In these, other source terms linked to homogeneous reactions have to be accounted for, as well as the divergence of fluxes. The expressions of fluxes differ in the porous and free medium, as diffusion, convection, and rarefied gas effects have different importances. A *total mass balance equation* may be solved, either as such, or by summing up all species mass equations. Convective fluxes are obtained through the solution of a *momentum balance equation*, which takes very different forms outside the porous medium (Navier–Stokes equation) and inside it (Darcy's law). Finally, an *energy balance equation* has to be solved in order to describe heat transfer. In the case of Joule effect heating, a last set of equations treating electromagnetism may be required, too.

This list of equations (mass, species, momentum, and energy) is the one usually encountered in classical computational fluid dynamics (CFD) codes, with some extra difficulties:

- The presence of a porous medium with possible rarefied gas effects implies the handling of specific models for the fluxes.
- The coupling between the porous medium and the surrounding fluid is a specific issue that can be addressed either by weak or by strong coupling approaches.
- The space/time evolution of the porous medium is a specific feature of CVI, requiring transient solution of the equations following the time scale of infiltration.

Depending on the aimed level of precision of the model, some parts of this set of equations may be subjected to simplifications.

Table 17.2 lists a complete set of balance equations, including resistive or inductive heating, all in steady-state except the densification equation. The equations involve the computation of several fluxes and source terms, which have to be described as laws, described in the right column. Note that a specific choice for the principal variables has been made: porosity, temperature, velocity pressure, partial pressures, and potentials for electromagnetism. Many other variable choices are possible, like using momentum instead of velocity, or partial densities instead of partial pressures, and so forth.

The boundary and interface conditions concern several types of boundaries. The most specific ones are related to mass, species, and momentum transfer. They are described in Table 17.3.

The provided equations and laws involve some properties of the fluid and/or of the porous medium, plus chemical rate constants. They are listed in Table 17.4, with their dependencies to other variables of the system. Because of these dependencies, nonlinearities may occur. Some of them are benign, but other ones may have deep effects, as for instance the Arrhenius laws. Moreover, all porous medium properties being functions of the porosity, cumulative effects are to be expected. Actually, as far as

Table 17.2 Balance equations and constitutive laws: species, mass, momentum, energy, and electromagnetism for heating

Quantity	Balance equation	Constitutive laws
Solid mass	Densification equation $\frac{\partial \varepsilon}{\partial t} = \frac{M_s}{\rho_s}\sigma_v R_{\text{het}}$	Heterogeneous reactions $R_{\text{het}} = \sum_{l=1}^{N_{\text{het}}} R_{i,\text{het}}$ $= \sum_{l=1}^{N_{\text{het}}} \left(\upsilon_{il} k_l \prod_j \left(\frac{P_j}{\mathcal{R}T}\right)^{\alpha_{lj}}\right)$
Species +momentum in porous medium	Transport-reaction equation $\nabla \cdot \left(\mathbf{J}_{i,V} + \mathbf{J}_{i,D}\right) = \epsilon R_{i,\text{hom}} + \sigma_v R_{i,\text{het}}$	Homogeneous reactions $R_{i,\text{hom}} = \sum_{l=1}^{N_{\text{hom}}} \left(\upsilon_{il} k_l \prod_j \left(\frac{P_i}{\mathcal{R}T}\right)^{\alpha_{lj}}\right)$ Viscous flux (Darcy) $\mathbf{J}_{i,V} = C_i \mathbf{v} = \frac{P_i}{\mu \mathcal{R}T} \underline{\underline{K}} \cdot (\nabla P - \rho \mathbf{g})$ Dusty-gas model $\sum_{j \neq i}^{n} \underline{\underline{D}} ij^{-1} \cdot \left(x_i \mathbf{J}_{j,D} - x_j \mathbf{J}_{i,D}\right)$ $-\underline{\underline{D}} iK^{-1} \cdot \mathbf{J}_{i,D} = \frac{\nabla P_i}{\mathcal{R}T}$
Mass and momentum in cavity	Continuity $\nabla \cdot (\rho \mathbf{v}) = 0$ Navier–Stokes $\nabla \cdot (\rho \mathbf{v}\mathbf{v}) + \nabla \cdot \underline{\tau} = \nabla P - \rho \mathbf{g}$	Perfect gas law; Dalton's law $\rho = \frac{P}{\mathcal{R}T} \sum_i^{N_{sp}} x_i M_i$; $P_i = x_i P$ Stresses $\underline{\tau} = -\mu \left(\underline{\underline{\nabla}} \mathbf{v} + {}^t\underline{\underline{\nabla}} \mathbf{v}\right) + \frac{2}{3}(\nabla \cdot \mathbf{v}) \underline{\underline{\text{Id}}}$
Species in cavity	Diffusion-convection-reaction $\nabla \cdot \left(\frac{P_i}{\mathcal{R}T}\mathbf{v} + \mathbf{J}_i^D\right) = R_{i,\text{hom}}$	Stefan–Maxwell $\mathcal{R}T \sum_{j \neq i}^{n} \left(\frac{x_i \mathbf{J}_{j,D} - x_j \mathbf{J}_{i,D}}{\mathcal{D}_{ij}}\right) =$ $\nabla P_i - \omega_i \nabla P - P \sum_{j \neq i}^{n} x_i x_j \alpha_{ij} \frac{\nabla T}{T}$
Energy	Heat equation $\rho c_p \mathbf{v} \cdot \boldsymbol{\nabla} T + \boldsymbol{\nabla} \cdot \mathbf{q_c} = S_h + S_r$	Fourier law $\mathbf{q}_c = -\underline{\underline{\lambda}} \cdot \nabla \mathbf{T}$ Heating $S_h = \frac{1}{2\sigma_{el}} \mathbf{j}_{el} \bar{\mathbf{j}}_{el}$ Thermochemistry $S_r = -\sum_{l=1}^{N_{tot}} \left(\Delta_{il} H k_l \prod_j \left(\frac{P_j}{\mathcal{R}T}\right)^{\alpha_{lj}}\right)$
Vector and scalar potentials	Maxwell equations $\nabla \times \left((\mu_0 \mu_r)^{-1} \nabla \times \mathbf{A}\right) = (\mathbf{j}_{el} + \mathbf{j}_s)$ $\boldsymbol{\nabla} \cdot \mathbf{j}_{el} = 0$	Ohm's law $\mathbf{j}_{el} = -\sigma_{el} \left(\frac{\partial \mathbf{A}}{\partial t} + \nabla V\right)$

Table 17.3 Boundary conditions for detailed reactor-scale CVI models

Boundary	Boundary conditions	Equations
Inlet	Fixed temperature	$T = T^{in}$
	Fixed velocity profile	$\mathbf{v} = \mathbf{v}^{in}(\mathbf{x})$
	Danckwerts BC's	$\left(\frac{P_i M_i}{\mathcal{R}T}\mathbf{v} - \sum_{j=1}^{n}\frac{M_i D_{ij}}{\mathcal{R}T}\nabla P_j\right)\cdot\mathbf{n} = \frac{P_i^{in} M_i}{\mathcal{R}T}\mathbf{v}^{in}\cdot\mathbf{n}$
	or fixed composition	$P_i = P_i^{in}$
Inner reactor wall	Stefan velocity	$\mathbf{v}\cdot\mathbf{n} = \rho^{-1}\sum_{i=1}^{n} M_i R_{i,\text{het}}$
	Species fluxes	$\left(\frac{P_i M_i}{\mathcal{R}T}\mathbf{v} - \sum_{j=1}^{n}\frac{M_i D_{ij}}{\mathcal{R}T}\nabla P_j\right)\cdot\mathbf{n} = M_i R_{i,\text{het}}$
Outlet	Fixed pressure	$P = P_{\text{ref}}$
	Null normal gradients	$\nabla(T)\cdot\mathbf{n} = 0,\ \underline{\underline{\nabla}}\mathbf{v}\cdot\mathbf{n} = 0\nabla(P_i)\cdot\mathbf{n} = 0$
Interface	Continuity of T and all P_i	$T^p = T^f,\ P_i^p = P_i^f$
	Equality of fluxes	$\mathbf{J}_i^p + (1-\epsilon)R_{i,\text{het}}\mathbf{n} = \mathbf{j}_{T,i}^f$
	Effective Stefan velocity	$\mathbf{v}^f = \rho^{-1}\sum_{i=1}^{n} M_i\left(\mathbf{J}_i^p + (1-\epsilon)R_{i,\text{het}}\mathbf{n}\right)$
Cavity walls	Radiative flux interchange	

Table 17.4 List of properties required for CVI modeling

Property	Depends on …	Relation
Free gas phase		
Viscosity	T, P_i	$\mu \approx T^{1/2}$
Thermal conductivity	T, P_i	$\lambda \approx T^{3/2}/P$
Binary diffusion coefficients	T, P_i	$\mathcal{D}_{ij} \approx T^{3/2}/P$
Reaction rate constants	T	$k_r \approx \exp\left(-\frac{E_a}{\mathcal{R}T}\right)$
Porous medium		
Internal surface area	Porosity ε	$\sigma_v(\varepsilon)$ nonmonotonous
Average pore diameter	ε, σ_v	$\bar{d}_p = \frac{4\varepsilon}{\sigma_v}$
Permeability	$\varepsilon, \bar{d}_p$	$\underline{\underline{K}} = \varepsilon\frac{\bar{d}_p^2}{32}\underline{\underline{\eta}}_v^{-1}(\varepsilon)$
Knudsen diffusivity	$T, \varepsilon, \bar{d}_p$	$\underline{\underline{D}}_{i,K} = \varepsilon\frac{\bar{d}_p}{3}\sqrt{\frac{8\mathcal{R}T}{\pi M_i}}\underline{\underline{\eta}}_K^{-1}(\varepsilon)$
Effective binary diffusivity	T, P, ε	$\underline{\underline{D}}_{ij} = \varepsilon\mathcal{D}_{ij}\underline{\underline{\eta}}_b^{-1}(\varepsilon)$
Heat conductivity	ε, T	$\underline{\underline{\lambda}} = f(\varepsilon)$
Electrical resistivity	ε, T	$\underline{\underline{\sigma}} = f(\varepsilon)$

porous media are concerned, accurate laws for these geometrical and transport-related properties as functions of infiltration progress are required. This is typically achieved with pore-scale modeling, as detailed in Section 17.5.

17.4.2 Numerical solution algorithms

Commercial software packages for aerothermochemistry are now rather mature, but their direct use for CVI modeling is not easy because they do not account for an evolving porous medium containing porosity gradients. The most popular numerical methods for continuity, Navier–Stokes, energy, and species balance equations are finite differences (FD), finite volumes (FV), and finite elements (FE).

Two types of solution algorithms may be proposed. On one hand, it may be attempted to merge the free-medium and porous-medium balance equations into a single formalism and then enter it either in a multiphysics software or in a CFD package under the form of user-defined fields and routines or in a custom, *ad hoc* solver. This is a "strong space coupling" approach. The solution of the balance equations may be simultaneous ("strong physical coupling") or iterative. The other possibility consists of physically separating the porous medium from the surrounding reactor cavity. Different numerical tools may be chosen for each domain; an iterative procedure has to be designed, so that alternating the resolution in both media ends up converging to a common result on the interface (see boundary conditions in Table 17.3). Typically, the partial pressures resulting from a free-medium computation are used as Dirichelt BCs on the porous medium, and fluxes resulting from the porous medium computations are used as Neumann BCs for the free medium. Descamps, Reuge, and Vignoles (Vignoles et al., 2000; Reuge and Vignoles, 2005) have successfully validated this type of procedure, after recognizing that under-relaxation may be necessary to avoid divergence.

17.5 Description of the porous media: Pore-scale modeling and up-scaling

Obtaining effective geometrical and transport properties from the description of the porous medium structure is a matter of up-scaling, homogenizing, or averaging, that is, some average has to be taken on the pore-scale physics up to a larger scale, allowing the replacement of a detailed structure by some homogeneous equivalent medium. A representative volume element (REV), therefore, has to be defined. Several methods are available for the extraction of effective coefficients by a change of scale:

- A first method is based on a description of the medium by n-point correlation functions (Hashin and Shtrikman, 1962; Torquato, 2002) and variational bounds may be produced; the trivial extremes are the series and parallel composite laws (Wiener, 1912).
- The homogenization technique (Bensoussan et al., 1978; Sanchez-Palencia, 1980) consists in a formal space scale separation. The detailed transfer equations are subjected to an asymptotic analysis in which the physical variables are decomposed into "large-scale" and "small-scale" components. The latter are linearized with respect to the former in order to provide

closure problems that can be solved analytically or numerically. The obtained averaged equations feature integrals over the small-scale closure variables that enter the expression of the effective transfer coefficients. Most results were obtained when applying this method to periodic unit cells (PUC), but care has to be taken that a PUC is usually much smaller than an REV. Indeed, due to the symmetries of the problems, the perturbations brought by the boundary conditions are cancelled, so that results on a PUC and on the REV are equal.

- The volume averaging technique (Whitaker, 1999) is similar to homogenization; the "large-scale" and "small-scale" components of the physical variables are recognized as an average and a perturbation, respectively. Averaging the detailed transfer equations and subtracting the obtained equations to the latter give rise to perturbation equations; again, linearizing the perturbations with respect to the large-scale variables yields closure problems. In many standard situations, the result of this technique is equal to the preceding one (Bourgeat et al., 1988).
- An apparently simpler method is a direct computation of a transfer problem in some REV, applying a gradient and recovering a flux. Then, the correlation of the flux to the gradient yields an identification of the transfer coefficient. Actually, when performed carefully, the computations are quite similar to the closure problem solutions of the preceding two methods.
- Another method relies on the solution of transient transfer problems by random walks (RW). Effective coefficients are obtained as covariances of the displacements or of the velocities (Einstein, 1956; Chandrasekhar, 1943; Melkote and Jensen, 1989; Kim and Torquato, 1990; Torquato and Kim, 1989). The time convergence of the coefficients usually corresponds to a characteristic dimension that can be understood as an REV size.

The application of any of these methods to porous media requires some description of its structure. The starting point is an image or a collection of images, in 2-D or 3-D. Evaluations may be performed either directly or indirectly, depending on the technique and on the level of detail contained in the image(s).

- A first technique consists of recognizing in the image some features and dimensions, and refer to ideal media, either periodic (e.g., square or hexagonal arrays of parallel cylinders) or random. The latter type of media is described either only by some statistical data, like averages, variances, and n-point correlation functions, or by collection of computer-generated images from which average results are obtained. This is more or less a "virtual material" approach.
- Another technique consists of performing numerical computations directly on the experimental images, usually after some image processing routines, like noise filtering and segmentations. In that case, we are dealing more with a "numerical material" approach.

We will review briefly these two techniques in the following sections.

17.5.1 Ideal models

For many years, the focus has been on the properties of ideal media, like random beds of cylinders, either fully overlapping or partially overlapping, or of capillaries. The methods were principally aimed at a separate evaluation of all geometrical and transport properties. They are listed in Table 17.5. In I-CVI, the main properties of interest are the internal surface area and the effective binary and Knudsen diffusivities: estimates for a variety of porous media have been obtained, using a Monte Carlo (MC)/RW technique (Sotirchos and Tomadakis, 1990; Melkote and Jensen, 1989, 1992; Vignoles, 1995); effective

thermal conductivities were computed by the same technique (Tomadakis and Sotirchos, 1993c). For F-CVI, permeability estimates have been assessed for a "node-bond" equivalent pore network (Starr, 1995); more recently, a method (Johnson et al., 1986) for the estimation of permeabilities from the knowledge of effective diffusivities has been tested and validated for a variety of fibrous media (Tomadakis and Robertson, 2005; Vignoles et al., 2007a). Skamser et al. (1994) have estimated both permeabilities and thermal conductivities for unidirectional fiber bundles, either from an ideal model or from computer-generated 2-D images.

17.5.2 Image-based models

In general, and except for permeabilities, the amount of numerical estimations exceeds by far the quantity of direct measurements; this is due to the working scale, which is very small. Nonetheless, direct imaging of the fiber arrangement in bundles and woven preforms gives a hint of how transport and reaction may take place. More explicitly, a direct numerical solution of the transport equations inside domains directly extracted from images allows obtaining effective coefficients.

For more complex structures, 3-D investigation can be performed, using in particular X-ray computerized microtomography (CMT; Coindreau et al., 2011). It has been used successfully to characterize the structure of how SiC fiber cloth layup preforms at macropore scale (pixel size of 15.6 mm) (Kinney et al., 1993; Lee et al., 1998). Carbon fiber preforms also have been examined at fiber scale and macropore scale (Coindreau and Vignoles, 2004). An image segmentation algorithm specific to phase-contrast images obtained with synchrotron X-rays on poorly absorbent materials like carbon has been developed to make it possible (Vignoles, 2001). The computation of geometrical parameters, such as surface area and pore size distribution, directly from the images, has been validated against experimental data (Coindreau and Vignoles, 2005). The fiber-scale results for binary and Knudsen diffusion were consistent with the estimates on similar ideal media (Tomadakis et al., 1992). A double change-of-scale strategy allowed integrating the fiber-scale results and comparing the macroscale values to experimental data, with satisfactory results on thermal conductivity (Coindreau et al., 2005), permeability, and Knudsen diffusivity (Vignoles et al., 2007a).

17.5.3 Pore-scale simulations of chemical deposition

The study of geometry and transport in families of ideal media has always rested on the idea that there was only one way for the properties to vary with porosity; usually some kind of "dilation" of the solid phase is the underlying assumption. However, actual CVI conditions usually imply some pore-scale diffusional limitations; this motivates further efforts at predicting the detailed geometrical evolution of complex porous media. Jin and Wang (2003) have developed a level-set method suited to such a simulation, assorted to a closed pore detection, and presented results in the kinetic limit in a small cubic arrangement of spheres. This method has been applied to the case of woven SiC fiber preforms by Guan et al. (2013). Schnack and his coworkers have developed a phase-field model involving the Ginzburg–Landau equations, first

Table 17.5 Computations of transport coefficients in porous media for CVI

References	Transport and reaction	Type of porous medium	Numerical method
Burganos and Sotirchos (1989)	Knudsen diffusion	1-D, 2-D, 3-D random overlapping cylindrical pores	MC/RW
Currier (1990)	Plain diffusion and surf. area	1-D random partially overlapping cylindrical fibers	
Tomadakis and Sotirchos (1991a)	Knudsen diffusion	1-D, 2-D, 3-D random overlapping cylindrical fibers	MC/RW
Tomadakis and Sotirchos (1991b)	Knudsen diffusion and surf. area	1-D random overlapping cylindrical fibers	MC/RW
Tomadakis and Sotirchos (1993b)	Knudsen to continuum diff.	Random network of overlapping cylindrical capillaries	MC/RW
Tomadakis and Sotirchos (1993a)	Transition to continuum diff.	Random fiber structures	MC/RW
Transvalidou and Sotirchos (1996)	Knudsen to continuum diff.	Square arrays of bundles with random 1-D cylindrical fibers	MC/RW
Tomadakis et al. (1992)	Knudsen to continuum diff.	1-D, 2-D, 3-D random overlapping cylindrical fibers	MC/RW
Sotirchos and Tomadakis (1990)	Gas transport and surf. area	1-D, 2-D, 3-D random overlapping cylindrical fibers	MC/RW
Melkote and Jensen (1989, 1992)	Knudsen to continuum diff.	3-D random overlapping cylindrical fibers	MC/RW
Vignoles (1995)	Knudsen to continuum diff.	Inter-tow pores – ideal geometries	MC/RW
Vignoles et al. (2007a)	Knudsen to continuum diff.	3-D X-ray CMT images of fibrous media	MC/RW
Tomadakis and Sotirchos (1996)	Conduction and continuum diff.	Random arrays of conductive cylinders dispersed in a conductive matrix	MC/RW

Table 17.5 Continued

References	Transport and reaction	Type of porous medium	Numerical method
Tomadakis and Sotirchos (1993c)	Conduction and continuum diff.	Random freely overlapping cylinders with various orientation distributions	MC/RW
Skamser et al. (1994)	Heat conduction viscous flow and surface area	1-D partially overlapping random fibers + discretized micrographs	Equivalent electrical circuit + "marker-and-cell" Stokes eq. solver (FD)
Starr (1995)	Viscous flow	Woven cloth stackings	Node-bond percolation
Tomadakis and Robertson (2005)	Viscous flow	1-D, 2-D, 3-D random overlapping cylindrical fibers	Analytical + correlation w/diffusion (Johnson et al., 1986)
Vignoles et al. (2007a)	Viscous flow	3-D X-ray CMT images of fibrous media	Finite volumes + correlation w/diffusion (Johnson et al., 1986)

for pyrolytic carbon deposition (Langhoff and Schnack, 2003, 2008; Ekhlakov et al., 2008), then for SiC deposition (Schnack et al., 2010; Zhu et al., 2011, 2013; Wang et al., 2013), and for both simultaneously (Zhu and Schnack, 2013). However, up to now this method has only provided results similar to single-pore analyses.

By adding sticking events to the walk algorithm, a "voxel filling" procedure, and a closed pore detector, the MC/RW diffusion simulator (Vignoles, 1995) has been turned into another pore-scale infiltration simulator (Vignoles et al., 2010a; Ros et al., 2011). This numerical method is related to the volume-of-fluid (VOF) technique. The fluid–solid interface has been discretized using an original simplified marching cube algorithm (Vignoles et al., 2011a). Application to large 3-D images has been demonstrated (Vignoles et al., 2011b). This simulation software has been used for a study of "infiltrability" of fibrous arrangements (Mulat, 2008), as illustrated in Figure 17.4. Three example images were taken from a CT scan and were segmented into fibers, matrix, and pores. Then, their infiltration history has been reconstituted by running numerical matrix deposition with different dimensionless parameters Kn and Φ (or Sh or Da). The set of parameters giving the least difference between the numerical matrix and the actual matrix has been retained. In this case, it was corresponding to a high value of Kn (i.e., rarefied gas regime) and a low value of Φ (i.e., a reaction-controlled regime). This "reverse engineering" approach allowed the identification of the processing parameters (low P, low T). The infiltration trajectories are plots of the open pore diameter as a function of the global pore volume fraction. Though the three samples have virtually the

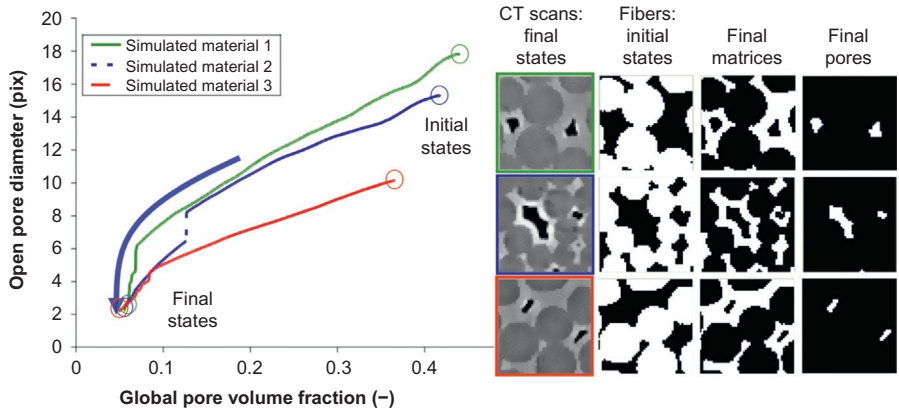

Figure 17.4 A comparative study of infiltrability in selected images. Right: CT scans and their segmentation in fibers, matrix, and pores. Left: numerical reconstitution of the densification trajectories: open pore diameter versus global pore volume fraction. The arrow indicates the direction of time evolution.

same end points (on the bottom left of the curves), it is possible to distinguish the most infiltrable one as having the slowest decrease of the open pore diameter when the total porosity diminishes, and it is indeed the one corresponding to the top image.

17.5.4 Homogenized CVI models using complex porous media representations

Sotirchos (1991) has developed a model for I-CVI, first in one dimension, using a full description of multicomponent diffusion and some structural models for porous medium effective properties; he used B-spline collocation for the numerical resolution. He could use this model to give some optimal pressures and temperatures (Ofori and Sotirchos, 1996a) and explore the influence of the structural models (Ofori and Sotirchos, 1996b). The model has then been extended to 2-D computational meshes, using FE for the resolution (Ofori and Sotirchos, 1997a).

Currier (1990) has developed an overlapping cylinders model based on a scaled particle theory, under the form of power law relationships with fitted exponents. They have inserted it into a 1-D solver for chemical vapor infiltration of carbon from methane in cylindrical fiber bundles (Currier et al., 1996). Favorable agreement is then seen between experimentally measured weight gain data and pseudo-steady-state calculations. The model also accounts for how the sensitivity to initial bundle porosity and accurately predicts final bundle porosities over a range of temperatures.

In the case of woven plies reinforcements, Chung, McCoy, Smith, and Cagliostro (Chung and McCoy, 1991; Chung et al., 1991, 1992, 1993) have developed a multiscale model, separating the intratow and intertow pore spaces in a PUC of the weaving/stacking pattern.

A tow-scale simulation algorithm (Vignoles et al., 2011c) has been developed using an MC/RW method, in which the porous medium is considered as a continuous

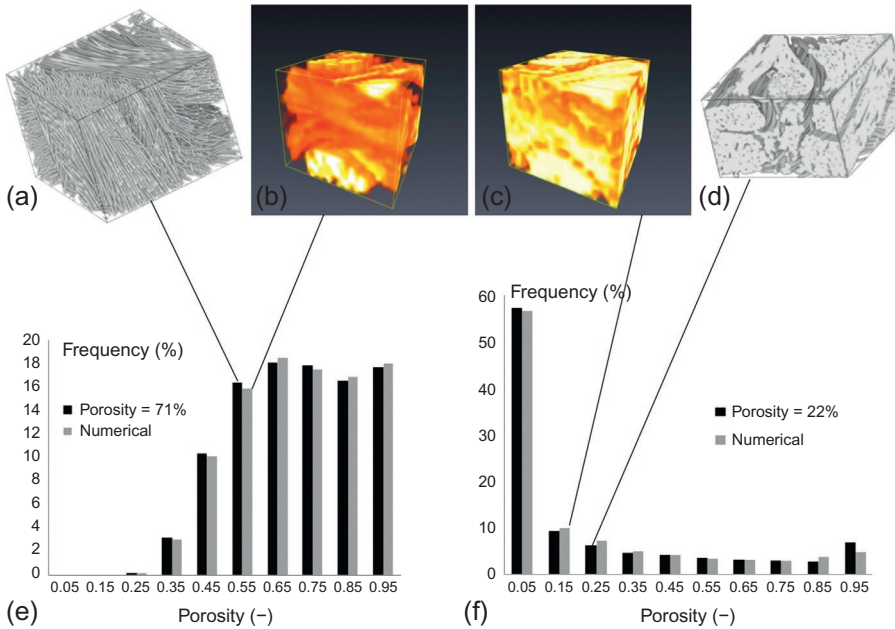

Figure 17.5 Validation of a tow-scale infiltration code (Vignoles et al., 2011c; Figure 17.4). Evolution of the porosity distribution during infiltration and comparison with experimental data. (a) Original high-resolution CMT scan of a raw preform, with 71% porosity. (b) Downscaled version of image (a). (c) Image (b) after numerical infiltration down to 22% porosity. (d) Original CMT scan of another sample of the same material, infiltrated experimentally down to 22% porosity. (e) Comparison of pore volume histograms before infiltration. (f) Comparison of pore volume histograms after infiltration.

field of anisotropic diffusion coefficient and of internal surface area. In addition, formation of sealcoat around the bundles was modeled simultaneously. The model has been validated on X-ray tomographic data as illustrated in Figure 17.5: A high-resolution CT scan of a fibrous preform has been transformed in a lower-scale resolution domain by downsampling. The relation between gray-scale levels and diffusion coefficients is based on correlations obtained on high-resolution (fiber-scale) diffusion and reaction simulations (Vignoles et al., 2007b) and a local fiber orientation detection routine that allows setting the local diffusion tensor axes along the fiber direction. A numerical infiltration run has been performed, and the final pore size distribution has been compared to a CT scan of an experimentally infiltrated sample. An excellent agreement has been found.

17.6 I-CVI of C/C composites

The most economically important fiber-reinforced ceramic composites are C/C composites; a large part of them is fabricated by CVI. Modeling is a direct aid here in reducing processing costs and increasing the final material quality. Therefore, a vast literature on

CVI modeling deals with the infiltration of hydrocarbons diluted in H_2; their reaction with the carbon fiber preform leads to the formation of a pyrocarbon (pyrolytic carbon) matrix. Its nanotexture and the overall deposit homogeneity deeply rely on processing parameters such as the gas composition, pressure, temperature, the residence time, or the reactor surface/volume ratio (Lieberman and Pierson, 1974; Lavenac et al., 2001a; Reznik and Hüttinger, 2002; Descamps et al., 2001a; Reuge et al., 2002; Vignoles et al., 2004). In turn, final composite thermomechanical properties and graphitizability are directly impacted by these characteristics (Oberlin, 1984). The specificity of pyrocarbon deposition arises from its particularly complex chemistry. Studies in this field have provided extensive knowledge of precursor gas decomposition. The cases of methane (Benzinger and Hüttinger, 1996, 1998, 1999a,b,c; Zhang and Hüttinger, 2001, 2002; Li and Deutschmann, 2007; Li et al., 2008; Norinaga and Deutschmann, 2007) and of propane (Lacroix et al., 2010; Ziegler et al., 2005a,b,c; Ziegler-Devin et al., 2007) have been treated thoroughly. The main point is that pyrolytic carbon deposition may occur from several hydrocarbons produced in the gas phase by thermal cracking. Hydrogen has been considered as a possible inhibitor of deposition, at least when using methane as a precursor. Moreover, the pyrolytic carbon nanotexture is known to depend on the composition of the local gas phase and on the surface/volume ratio (Vignoles et al., 2012). CVD on planar substrates was frequently used in order to identify the deposition kinetics. Global models embodying these results, plus the evolution of geometrical characteristics and transport properties of a preform at various infiltration stages, have been developed in order to optimize the final composite density as well as deposit homogeneity. Deposition from propylene has been considered first by FD with a simple kinetic model (Hou et al., 1999; Li et al., 2000), then with multistep kinetics (Li et al., 2005). Fuzzy neural networks have been used to optimize infiltration conditions (Li et al., 2003, 2004). Multistep models were used successfully for methane, too (Li and Deutschmann, 2007; Li et al., 2008). More complete models featuring a coupling with the external gas phase (McAllister and Wolf, 1993; Ibrahim and Paolucci, 2011) allowed the prediction of deposition gradients in a whole reactor containing numerous preforms.

Infiltration from propane in needle-stitched woven carbon fiber preforms has been addressed with an integrated strategy as described in Figure 17.3. This numerical effort combines the prediction of both matrix nanotexture and deposition thickness. It first consists of a chemical model describing relevant homogeneous and heterogeneous reactions leading from the precursor pyrolysis to pyrocarbon formation (Reuge et al., 2002; Vignoles et al., 2004, 2008). A two-scale infiltration model (Vignoles et al., 2010b,c, 2011b,c) is used for the computation of transport and geometrical properties of the preform at different description levels. These data are integrated to a reactor scale model (Vignoles et al., 2013) for the simulation of precursor decomposition, species transport, preform morphology evolution, and matrix nanotexture.

17.6.1 Modeling strategy

The modeling strategy is decomposed into four steps as shown in Figure 17.6. The construction of the final reactor scale tool requires the outputs produced by the first three numerical models. First, it must feature a semidetailed mechanism for propane

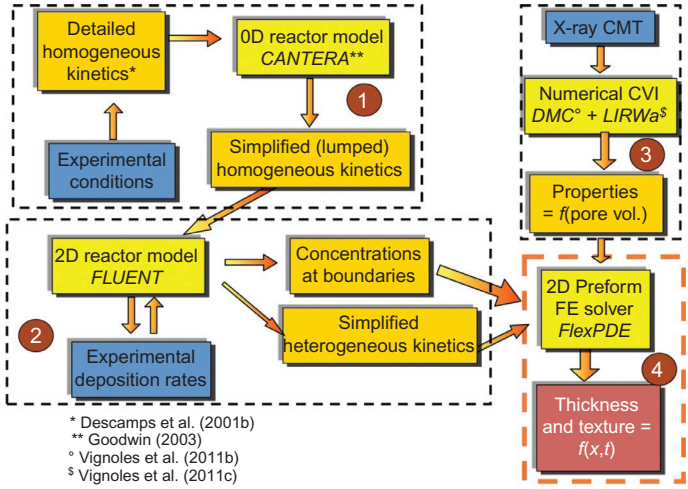

Figure 17.6 Model strategy for the I-CVI of pyrocarbons from propane.

pyrolysis (Descamps et al., 2001b). There are 41 species (from C1: CH_4, CH_3, etc., to C10: $C_{10}H_8$) and 133 reactions in this mechanism. This mechanism has been validated against experimental hot-wall CVD data (Descamps et al., 2001a,b; Féron et al., 1999; Lavenac et al., 2001b; Vignoles et al., 2004). In order to perform subsequent CVI computations, the reaction scheme is simplified, with a few lumped species and apparent reactions (Vignoles et al., 2008, 2013), as shown in Figure 17.7. Using the CANTERA software (Goodwin, 2003), the applied pressure and temperature are imposed to the gas phase, and species concentrations are computed as a function of time. The gas-phase maturation phenomenon is evidenced: the initial decomposition of propane gives first-generation species, principally C1 (methyl radical) and C2 (ethane, ethene); later on, acetylene and benzene appear; finally, higher molecular-weight species such as naphthalene occur. Homogeneous reaction rates are identified by the combination of this data and of the simplified scheme expressions.

The incomplete kinetic model is then introduced into the FLUENT CFD solver and a mass, heat, and momentum analysis in a 2-D axisymmetrical reactor is performed. The heterogeneous reaction rates are fitted by comparing numerically obtained deposition rates, for every set of operating conditions, with results from CVD experiments. When doing so favorably, concentration profiles of each species at the boundaries of the porous medium are also collected. The complete kinetic scheme may then be introduced in the final preform-scale 2-D axisymmetrical mass balance FE solver for preform consolidation. Gas transport may rely on viscous flow, ordinary (binary) diffusion, and rarefied gas flow (Knudsen diffusion) (Goodwin, 2003). In the present case, because the gases may freely flow around the porous sample, no appreciable pressure buildup appears; consequently, viscous flow is rather negligible with respect to the other transport modalities, as usual in isothermal CVI. Prior to simulation, the effective diffusivities and the internal surface area, given as functions of the pore

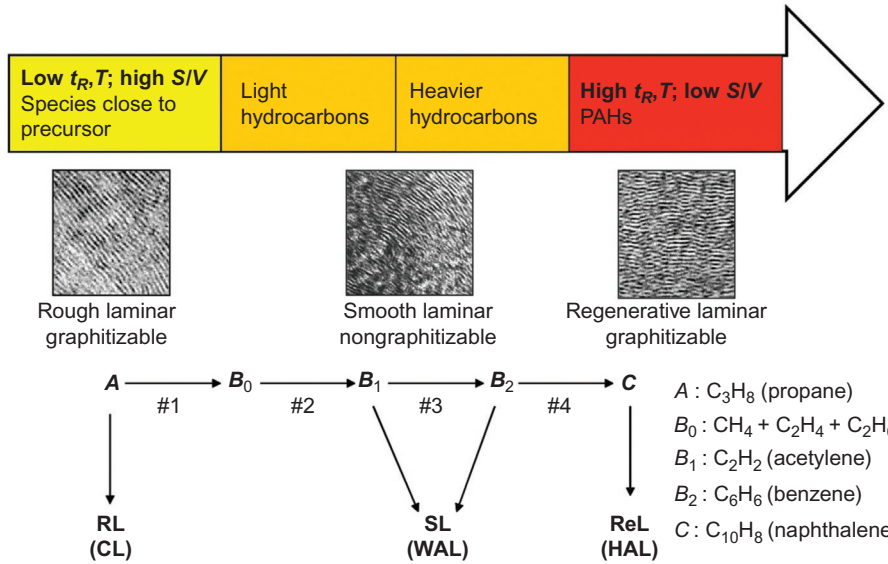

Figure 17.7 Simplified (lumped) kinetic scheme for the deposition of pyrocarbons from propane.

volume fraction, have to be determined. In this goal, the 3-D CMT images and the image-based infiltration models have been used. Deposit growth has been simulated in the high-resolution scans by using a homemade MC/RW algorithm dedicated to fiber-scale computations (Vignoles et al., 2011b). With this same tool, blocks representing different infiltration stages have been processed for the determination of the internal surface area and of the effective binary and Knudsen diffusivities (Coindreau and Vignoles, 2005; Coindreau et al., 2011; Vignoles et al., 2007a, 2011b). The determined laws were then inserted into another homemade MC/RW software suited to infiltration at the composite scale (Vignoles et al., 2011c). The resulting macroscopic scale laws are then inserted into the final reactor scale solver.

17.6.2 Results and validations

Validations have been sought against experimental data obtained in a hot-wall I-CVI setup, using two very distinct types of porous media: either fibrous preforms of C/C composites (Le Poche et al., 2005) or carbon foams (Vignoles et al., 2008), with a much lower σ_v ratio. Numerical simulations were performed following the described methodology for each preform and for the same experimental parameters (Vignoles et al., 2013). Table 17.6 proves that, whatever the physicochemical conditions, agreement between experimental and numerical results is obtained. The predominant nanotexture in each area is defined by studying the ratio of the deposition rates. In the case of sample P5-3, Figure 17.8 confirms that ReL pyrocarbon is present at the surface of the composites, whereas the proportion of SL pyrocarbon is higher at the center of the material.

Table 17.6 Experimental and computed deposit thicknesses and nanotextures (Vignoles et al., 2013)

Expt #	Pressure (kPa)	Res. time (s)	Duration (h)	Thickness (μm)		Nanotexture	
				Exptl.	Num.	Exptl.	Num.
				(First value: border; second value: center)			
Fibrous preforms: stitched woven fabric plies, $\sigma_v \approx 50{,}000$ per m							
P5-1	5	0.1	28 h 30 min	12–7	12–5.5	SL–RL	SL–RL
P5-2	5	0.35	18 h	6–3	6–3.5	SL–SL	SL–SL
P5-3	5	3	15 h	13–3	13–4.5	ReL–SL	ReL–SL
P2-3	2	3	14 h 30 min	4–1	4–2.5	ReL–SL	ReL–SL
P0.5-1	0.5	0.065	22 h	4–1	4.5–1.5	RL–RL	RL–RL
Fibrous preforms: carbon foams, $\sigma_v \approx 2000$ per m							
F1	5	0.2	19 h	25–25	26–26	SL–SL	SL–SL
F2	5	3	11 h 55 min	37–70	37–55	ReL–ReL	ReL–ReL

Samples P5-1, P5-2, and P5-3 were processed under the same pressure but different operating residence times. The increase of this quantity favors deposition at the surface of the preform and enhances obstruction of its center to gas access, as illustrated by Figure 17.8 and Table 17.6. This is due to the larger gas-phase maturation prior to entering the preform—more reactive species are created, and they deposit themselves very quickly at the pore entrances. Their molecular weight is higher, and their deposition mode is more condensation-like, yielding ReL, a highly textured pyrocarbon. Samples P5-1 and P0.5-1 were prepared for similar values of the residence time. The lower pressure applied to the latter induces a weaker deposition rate but delays the porous medium obstruction. Moreover, the deposited pyrocarbon is RL, has a high degree of anisotropy because it originates from a defect-free lateral growth mechanism. P0.5-1 represents the best infiltration conditions. At a given temperature, matrix properties are a result of a compromise between the pressure and the residence time. The nanotexture can be controlled through the latter; weak and important values favor formation of highly anisotropic pyrocarbons yielding better mechanical properties. However, this same quantity accelerates deposition at the surface of the preform, quickly obstructing its center to the gas phase. This phenomenon can be counteracted by lowering the pressure, therefore reducing the deposition rates and extending the infiltration duration.

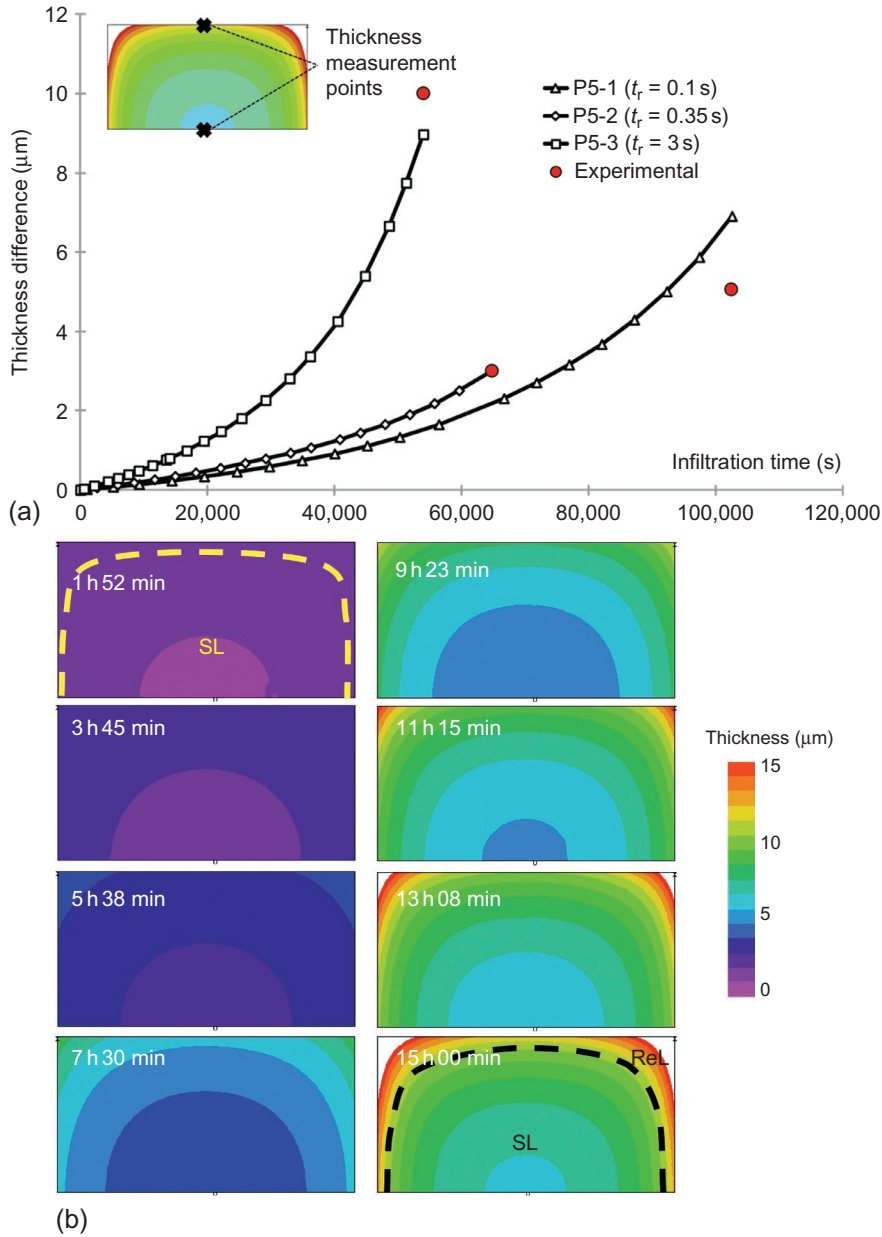

Figure 17.8 (a) Time evolution of infiltration gradients (thickness differences at points indicated in the inset) within the fibrous arrangements. (b) Time evolution of deposit thickness and nanotexture for experiment #P5-3.

17.7 I-CVI of CMCs

As opposed to C/C composites, CMCs more frequently have a more regular preform architecture. For instance, CMCs designed for civil jet engine hot parts (Cavalier et al., 2006), with excellent lifetimes, are constituted of a woven/interlocked 3-D arrangement of SiC fiber tows, infiltrated by a matrix, possibly multilayered in the case of self-healing CMCs (Goujard et al., 1995; Christin, 2005). Moreover, the matrix deposition kinetics usually displays less complex—but probably less well known—behavior than for carbon deposition. This is at least the case for SiC deposition, for which a one-reaction, first-order chemical kinetic scheme (Schoch et al., 1991; Brennfleck et al., 1984; Besmann et al., 1990; Guan et al., 2013) has been used and abused. As the deposition kinetics is rather fast, important depletion effects are to be expected. Accordingly, the effect of the gases surrounding the preform has been studied with particular care, first by Vignoles et al. (2000) and Reuge and Vignoles (2005), then by Wei et al. (2006a,b, 2007, 2008) who also discussed the effect of the reactor walls.

Due to the bimodal nature of the pore space (intratow/intertow), two-scale simulation approaches have been developed. The first works were due to Chung and McCoy (1991) and Chung et al. (1991, 1992, 1993). Kulik et al. (2004) have designed a model in which concentrations in both types of pores are distinct unknowns with exchange coefficients. For C/SiC composites preparation, Hua et al. (2009) considered a two-process model in which first the intratow pore space only is filled, then, after sealing, the sealcoat deposition over the bundles is the only phenomenon. More recently, Guan et al. (2011, 2013) have developed two-scale models for woven SiC/SiC composites infiltration.

In contrast with these models in which porous medium properties are essentially obtained from ideal models, two-scale image-based simulations have been developed recently (Vignoles et al., 2014a,b). In the following, we will present the methods that have been developed and discuss some results.

17.7.1 Strategy and numerical implementations

Keeping in mind the idea of handling simultaneously actual and virtual representations of the material, the strategy is articulated as shown in Figure 17.9.

The starting point is the acquisition of morphological information by 2-D and 3-D imaging. Images are available at low and high resolutions, that is, at fiber scale and yarn scale. 3-D CMT scans are of course a choice source of data, but micrographs taken in 2-D are very useful too. From this raw material, two processing routes are possible (Couégnat et al., 2012). The first one (plain lines) is to perform pattern recognition, recover the objects (yarns at large scale and fibers at a smaller scale), then to produce statistical data from them for further image synthesis or retain them as a 2-D or 3-D mesh for physicochemical and mechanical computations. The other way (dashed lines) is to extract image statistics directly without any pattern recognition and go to image synthesis with only this type of data as constraints.

Taking advantage from the experience acquired on C/C composites processing (see the preceding section), a two-scale approach has been developed, based on 3-D images

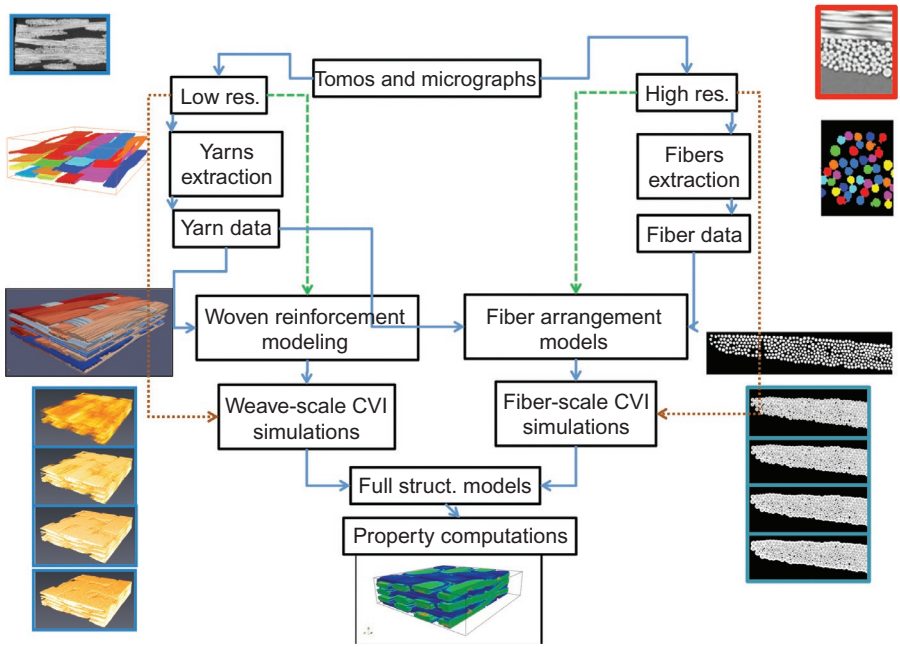

Figure 17.9 Scheme of the overall two-scale analysis and modeling strategy for CVI in woven preforms.

discretized on a regular voxel grid, as obtained by X-ray CMT (Coindreau et al., 2011) or by synthesis (Couégnat et al., 2012). An intratow code allows for the precise simulation of the matrix deposition (Vignoles et al., 2009); the deposit thickness variations are shown to depend on (i) the diffusion-reaction competition, which implies a smaller deposit thickness in small pores and (ii) the pore network connectivity. The results are interpreted as local laws for effective parameters (diffusivity, bulk reactivity) (Vignoles et al., 2010a) in the large-scale solver based on the Brownian motion (Vignoles et al., 2011c), capable of simultaneously computing the matrix phase amount in the tows and the sealcoat matrix thickness outside the tows. This code takes into account the local values of the volume fraction and of the orientation of the fibers.

17.7.2 Results and validations

The potentialities of the approach have been demonstrated by comparing the infiltrability of two types of woven reinforcements containing a preimpregnated ceramic obtained by slurry impregnation and pyrolysis (SIP) (Vignoles et al., 2014a). Figure 17.10 summarizes the comparative evolution of matrix infiltration in these two predensified textures. It can be clearly seen that the matrix thickness profile is more marked in the first case than in the second one, revealing a much lesser infiltration ability (or "infiltrability").

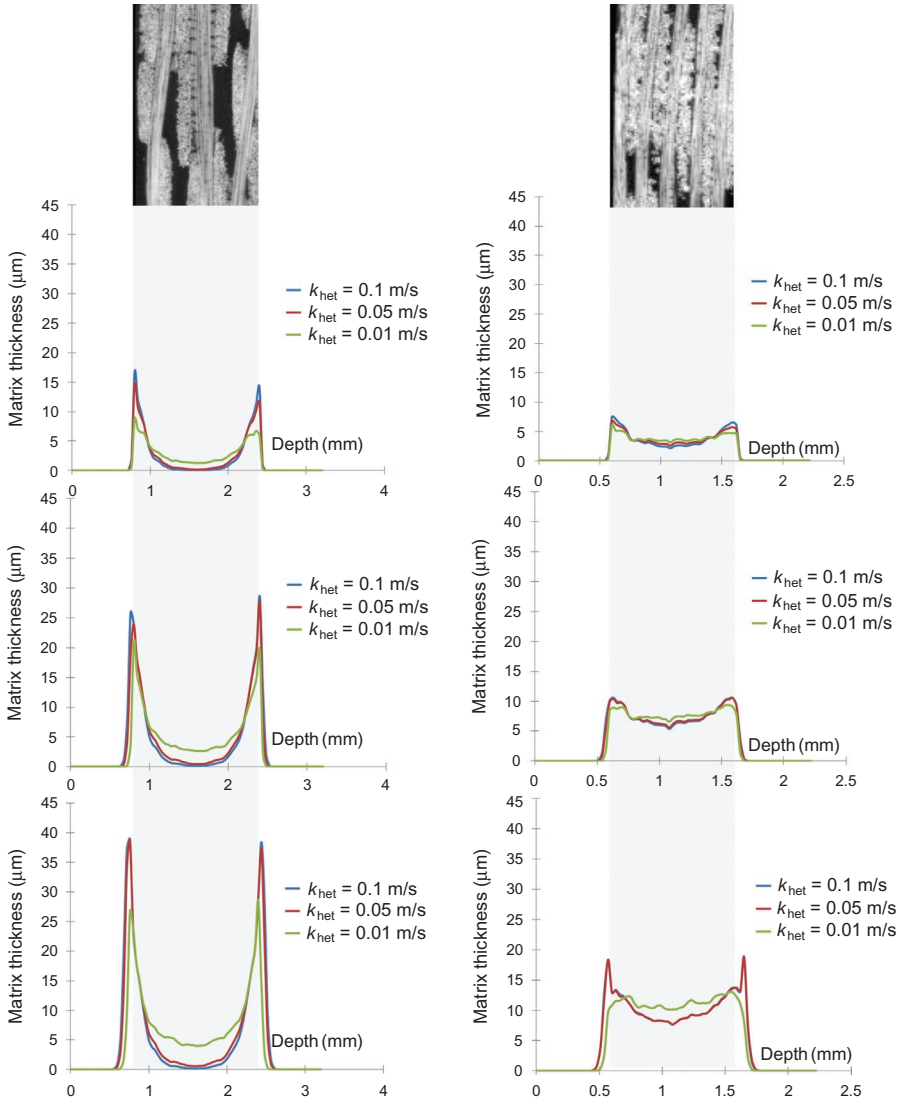

Figure 17.10 Infiltration profiles for two different woven reinforcement architectures (Vignoles et al., 2014b). Top: 5% added matrix volumes; middle: 10% added matrix volume; bottom: 15% added matrix volume. Three rate constants for heterogeneous deposition rate (k_{het}) were considered: 0.1 (blue), 0.05 (red), and 0.01 m s^{-1} (green).

These tools have the benefit of being usable on virtual images of fibrous architectures for the design of better materials, either for infiltrability or for further property computations, like mechanical or thermal. This completes a "virtual material" toolbox (Couégnat et al., 2012) aimed at evaluating the potentialities of material and/or process variations without actually fabricating test samples.

17.8 Variations of CVI

I-CVI has at least two drawbacks: its operation is lengthy and it is subject to premature pore plugging. A variety of CVI modifications have then been designed in order to overcome this limitation (Golecki, 1997). Most of them rely on the use of a thermal gradient and/or a pressure gradient; pulses of the operating conditions have also been considered. We will review first the thermal-gradient (TG-CVI) method, then the forced (F-CVI) and the pulsed (P-CVI) modifications.

17.8.1 TG-CVI, including film-boiling CVI

Theoretical investigations of thermal-gradient CVI have been carried out in various directions. They are either 1-D or 2-D and account for heat transfer by various ways: imposed boundary temperatures, constant power distributions, or preliminary solving of Maxwell's equations, while heat losses are represented by convective and/or radiative heat exchange boundary conditions. Various chemical systems have been also used. Table 17.7 is an attempt to compile several of these references.

These studies have first shown that inside-out temperature gradients could potentially favor a complete densification and that the total processing time may well be diminished with respect to I-CVI. However, it is shown that minimal temperature gradients are necessary to ensure the desired situation. In Melkote and Jensen (1990), Gupta and Evans (1991), Morell et al. (1992a), Midha and Economou (1997), Leutard et al. (2002), and Golecki et al. (1996), computations are shown where the correct situation is obtained at the beginning of densification, and the outside-in situation later appears. This rather frequent situation is schematized at Figure 17.11. On the other hand, reports on thermal gradient, forced CVI (Vaidyaraman et al., 1995), and on the "film-boiling" process (Rovillain et al., 2001) have mostly shown well-infiltrated materials. In this case, a densification front seems to exist at the beginning and until the end of the process. However, the latter process has other drawbacks, chiefly the strong energy consumption that underlies the presence of extreme gradients, and the necessity to handle flammable liquids together with a strong energy source.

A detailed modeling study was carried out on this "film-boiling" or "Kalamazoo" or "rapid densification" process and validated with respect to experimental results (Lines et al., 2005; Vignoles et al., 2006). It appeared that it is indeed an extreme case of TG-CVI, in which the temperature gradient is kept very high by maintaining the outer cold side at the precursor boiling temperature. Summing up its results and former works, it is appeared that the central point in TG-CVI is the control of the existence of the densification front. A mathematical study (Vignoles et al., 2005; Nadeau et al., 2006) has shown that there are only two independent parameter sets that control the front, and that in the 2-D parameter space, there is a front existence domain, sketched in Figure 17.11b. The front existence is indeed linked to the following criterion: the mass flux must be at least equal to what the chemical reaction needs (lower branch of the frontier); however, it is itself limited by diffusion (upper branch of the

Table 17.7 Comparative presentation of previous modeling works on isobaric TG-CVI

References	Heating	Cooling	Chemical system
1-D models			
King (1994)	Linear T profile		$(CH_3)_2SiCl_2 \rightarrow SiC + CH_4 + 2HCl$
Skamser et al. (1997)	Fixed inner temperature	Conv. and rad.	$3CO_2 + 3H_2 + 2AlCl_3 \rightarrow Al_2O_3 + 6HCl + 3CO$
Kawase et al. (1994)	Fixed inner temperature	Conv. and rad.	$2Al(OiPr)_3 + 6H_2 \rightarrow Al_2O_3 + 6C_3H_8$
Gupta and Evans (1991)	Constant power	Convective	$CH_3SiCl_3 \rightarrow SiC + 3HCl$
Morell et al. (1992a)	Constant power	Conv. and rad.	$CH_3SiCl_3 \rightarrow SiC + 3HCl$
Morell et al. (1992b)	Power = f(time)	Conv. and rad.	$CH_4 \rightarrow C + 2H_2$
Ofori and Sotirchos (1996a)	Microwave (analytical)	Conv. and rad.	$CH_3SiCl_3 \rightarrow SiC + 3HCl$
Morell et al. (1993)	Maxwell's equations	Conv. and rad.	$CH_3SiCl_3 \rightarrow SiC + 3HCl$
Melkote and Jensen (1990)	Fixed inner temperature	Fixed outer temperature	$CH_3SiCl_3 \rightarrow SiC + 3HCl$
Vignoles et al. (2006)	Fixed inner temperature	Boiling precursor	$C_6H_{12} \rightarrow C +$ by-prod.
2-D models			
Evans and Evans (1993)	Microwave (analytical)	Convective	$CH_3SiCl_3 \rightarrow SiC + 3HCl$
Tilley and Kriegsmann (2001)	Microwave (analytical)	Conv. and rad.	$CH_3SiCl_3 \rightarrow SiC + 3HCl$
Midha and Economou (1997, 1998)	Maxwell's equations	Conv. and rad.	$CH_4 \rightarrow C + 2H_2$
Leutard et al. (2002)	Maxwell's equations	Conv. and rad.	$CH_4 \rightarrow C + 2H_2$
Vignoles et al. (2006)	Fixed inner temperature	Boiling precursor	$C_6H_{12} \rightarrow C +$ by-products

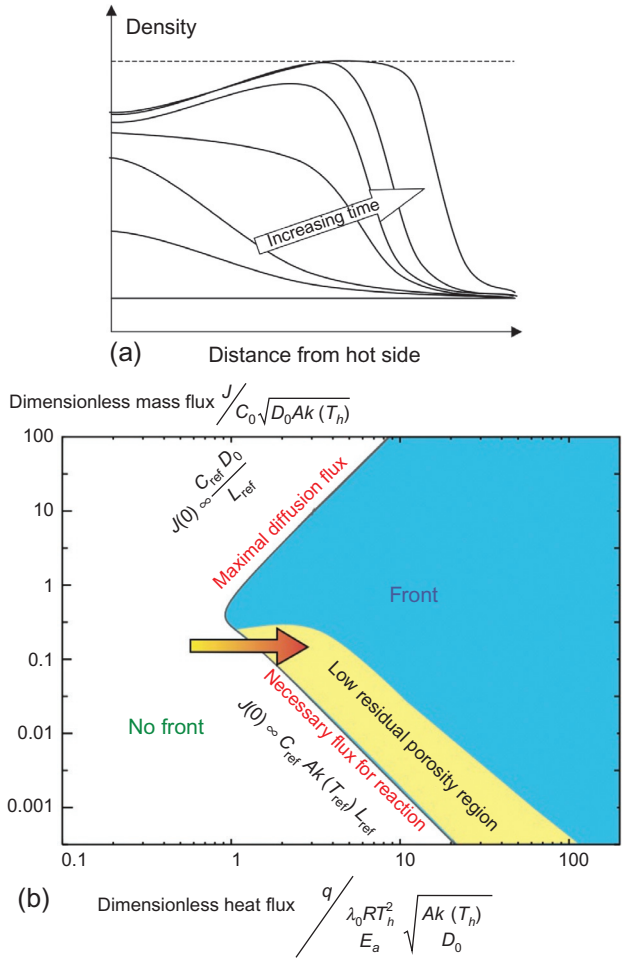

Figure 17.11 (a) A typical undesired thermal-gradient CVI scenario. (b) Parameter existence domain for a densification front in CVI with thermal gradient. The arrows on both graphs indicate the same evolution during the process, with an increase of the thermal gradient (Vignoles et al., 2005).

frontier). Because the amount of reaction and diffusion fluxes is computed with respect to a length scale that is natural to the problem,

$$L_f = \frac{\lambda_0 T_h}{q} \frac{\mathcal{R} T_h}{Ea} \tag{17.5}$$

(where T_h is the hot-side temperature, and λ_0 is the solid-phase heat conductivity), then there exists a minimal heat flux q that allows fulfilling the mass flux criterion, such that the Thiele modulus defined at Equation (17.3) with $L = L_f$ is unity.

This means that the critical flux decreases when (i) the activation energy increases, (ii) the gas diffusion coefficient increases (with a pressure decrease unless a Knudsen regime is attained), (iii) the hot-side temperature decreases, (iv) the solid-phase conductivity decreases, and (v) the fiber diameter increases (as $\sigma_v \propto d_f^{-1}$). The diagram in Figure 17.11b helps to understand how the undesired infiltrations in Figure 17.11a appear: when processing starts, the heat gradient is not strong enough and the critical condition for q is not fulfilled. Later on, the heat flux increases and eventually traverses the existence boundary, as shown by the arrow on the diagram. Also, it has been shown that the residual porosity tends to zero when the system lies close to the lower frontier of the existence diagram. In practice, it will be difficult to distinguish between such a behavior and a total infiltration. In this case, the velocity is approximately equal to L_f/τ (where τ is given by Equation 17.4), and in any case the front width is roughly equal to L_f (Vignoles et al., 2005). A 1-D analytical study by classical linear perturbation theory has produced a transverse stability condition that is usually fulfilled in practice but could not be in the case of very large preforms (as compared to the front thickness) (Vignoles et al., 2007c).

17.8.2 F-CVI

Forced-CVI has been studied either in isothermal or thermal-gradient conditions, the latter being more extensively employed for obvious reasons of better infiltration uniformity, as concluded from isothermal studies. Table 17.8 summarizes this literature.

Simple models are produced by alteration of Equation (17.1), inserting a convective term,

$$\frac{\partial}{\partial z}\left(r_p^2\left(uC - D_p\frac{\partial C}{\partial z}\right)\right) = -2r_p k_{\text{het}} C \tag{17.6}$$

with a velocity given by Darcy's law,

$$u = -\frac{B}{\mu}\frac{\partial p}{\partial z} \tag{17.7}$$

Solutions neglecting the effect of diffusion are functions of a dimensionless number, the Damköhler number of the first kind,

$$Da_I = \frac{\sigma_v k_{\text{het}} L}{u} \tag{17.8}$$

where μ is the gas viscosity, B is the porous medium permeability, and p_e is the exit pressure. An analogy may be performed with nonforced CVI by considering a modified Thiele modulus (see Equation 17.3) where the in-pore diffusion coefficient D_p is replaced by its viscous-flow equivalent (Ofori and Sotirchos, 1997b):

Table 17.8 Comparative presentation of models for F-CVI

References	Setup	Chemical system	Comments
1-D models			
Starr and Smith (1992b)	Isothermal	$CH_3SiCl_3 \rightarrow SiC + 3HCl$	Analytical
Roman (1994) and Roman et al. (1995)	Isothermal	$CH_3SiCl_3 \rightarrow SiC + 3HCl$	FD, single pore
Tsai and Desu (1991)	Isothermal	$CH_3SiCl_3 \rightarrow SiC + 3HCl$	FE, single pore
Kim et al. (2004)	Isothermal	$CH_3SiCl_3 \rightarrow SiC + 3HCl$	FD
Vaidyaraman et al. (1996) and Lewis et al. (1997)	Thermal gradient	Pyrolytic carbon	FD
Ofori and Sotirchos (1997c)	Isoth. and therm. grad.	$CH_3SiCl_3 \rightarrow SiC + 3HCl$	Collocation reversible deposition kinetics periodic flow reversal
2-D models			
Tai et al. (1994)	Thermal gradient	$CH_3SiCl_3 \rightarrow SiC + 3HCl$	Several kinetics schemes
Tai and Chou (1989, 1990a,b)	Thermal gradient	$CH_3SiCl_3 \rightarrow SiC + 3HCl$	Periodic sample reversal
Starr and Smith (1990, 1992a), Starr et al. (1991), Starr (1988), Besmann et al. (1995), Stinton et al. (1995), Jones and Starr (1995) and Probst et al. (1999)	Fixed thermal gradient	$CH_3SiCl_3 \rightarrow SiC + 3HCl$	2-D axi, FV
Ofori and Sotirchos (1997b)	Isoth. and therm. grad.	$CH_3SiCl_3 \rightarrow SiC + 3HCl$	FE

$$\Phi_v \approx Da_I^{1/2} = L\sqrt{\frac{\sigma_v k_{\text{het}} \mu}{B p_e}} \tag{17.9}$$

Again, values of Φ_v above unity lead to catastrophic density gradients; optimal values of the pressure differences may be worked out for a given set of conditions, that is, a given value of Φ_v. Pushing the analogy further, one can easily make use of the thermal-gradient results summarized in Figure 17.11 by replacing the diffusion coefficient D_p everywhere with its viscous flow analogue Bp_e/μ (Vignoles, 2006).

One of the most remarkable numerical efforts in CVI design has been the GTCVI software (Starr and Smith, 1990, 1992a; Starr et al., 1991; Starr, 1988; Besmann et al.,

1995; Stinton et al., 1995; Jones and Starr, 1995; Probst et al., 1999). Validated on I-CVI and F-CVI (Starr et al., 1993), it has allowed optimizing the processing parameter history during infiltration cycles (Starr and Smith, 1992a; Starr et al., 1991). Thanks to the model, the pressure drop can be utilized as an indicator of progress. The computed time evolution of the density inside the preform shows an interesting effect: because deposition occurs preferentially in regions where it has not yet taken place, the initial density gradients are progressively leveled. This has been termed "self-optimization" (Starr and Smith, 1990) but is actually an infiltration front phenomenon, similar to the TG-CVI situation mentioned in the previous section. This software has been used for scale-up of the F-CVI process (Besmann et al., 1994) and for application to tubular geometries (Stinton et al., 1995); accuracy of its predictions as checked with respect to X-ray CT scans of the infiltrated samples.

In their 2-D study, Ofori and Sotirchos (1997c) have shown that in the presence of thermal gradients, complex densification patterns may develop. They can show maxima in the interior of the preform and enlarge the region where strong multidimensional effects are present. The key factor that controls the appearance and extent of these effects is the distribution of flow over the entrance face of the preform. Design of this region is therefore crucial for the final material homogeneity.

17.8.3 P-CVI

Pressure-pulsed CVI (P-CVI) has also been modeled (Ofori and Sotirchos, 1996c; Sotirchos, 1991; Morell et al., 1992b), and the beneficial effect of an optimal pressure pulse frequency on the infiltration uniformity has been illustrated. Sotirchos (1991) has shown on the basis of a 1-D CVI model with full multicomponent, intermediate regime diffusion, and linear SiC deposition kinetics from MTS that optimal center/surface conversion ratios and better infiltration times may be found, if the resistance to convective transport is smaller than the resistance to diffusive transport. As a consequence, infiltrating homogeneous media with very small pores by P-CVI are not beneficial. Enriching the preceding model with a simultaneous solution of the complex Poisson equation for heating simulation, Ofori and Sotirchos (1996c) have explored the potential of simultaneous pressure pulsing and microwave volume heating. When rectangular wave pressure pulses are applied, density gradients are localized close to the preform exterior; using microwave heating helps dramatically in reducing selectively the deposition rate in this region, preventing premature pore plugging. Such a concept had been previously idealized, but with a different way of achieving the correct temperature distribution in the preform. The so-called "TP-CVI" (temperature and pressure pulsed CVI) process (Bertrand et al., 1998) works by periodically removing the sample from the hot zone it lies in. During the transient period that follows, the surface region is colder, and infiltration is favorable. Then, the gas feed is shut, the sample is inserted again in the hot zone, and the pressure is lowered. After this "purging" period, the cycle is resumed. Numerical modeling of the temperature history, validated with respect to experimental measurements, helped in working out a criterion for inside-out infiltration.

17.8.4 R-CVI

Reactive vapor infiltration has been scarcely modeled; however, Adjerid et al. (1995) have proposed a complete and consistent 2-D FE model at the largest scale (i.e., the whole part), in the case of Mo silicidation by Si vapor, and validated their study with respect to experiments described by Patibandla and Hillig (1993). They further proposed a multilayer model including explicitly the different possible silicides (Hillig et al., 1996).

17.9 Summary and outlook

This chapter has summarized a large literature on the modeling of CVI and its principal variations. Original physicochemical couplings have been identified and specific methods have been designed to tackle them. Analytical and simple numerical models have illustrated the main features of the process, with a particular focus on the problem of premature pore plugging, as a function of some experimental parameters. Optimizations have been proposed in many directions, based on these models. The thermal gradient, forced, and pulsed variations of the process have been investigated and it has been shown that they may help removing the principal drawbacks of the baseline process.

The ever-increasing access to intensive numerical facilities has enabled the development of several detailed, all-inclusive models. In addition, the access to nondestructive 3-D characterization has allowed very realistic multiscale image-based modeling. The gap between applied mathematics and process engineering has been bridged to a large extent; however, there is still room for interesting, elaborate analytical models.

Even today, this rather mature domain is still of interest, for several reasons. First, the industrial application of CVI is principally thermostructural composite fabrication, and the market for these materials is significant, imposing an international race for better process efficiency. Second, the fundamental physicochemical phenomena taking place in the process are very complex and intricate, and still deserve more accuracy in their description.

Future trends in CVI modeling include

- Extensions to a better description of the gas-phase chemistry in well-known systems such as SiC deposition from chlorosilanes. There is still plenty of room for investigation of the interplay between transfer phenomena and the numerous, highly nonlinear reactions taking place during the process.
- Incorporation of new kinetic schemes for the deposition of other refractory carbides, borides, and nitrides that are still poorly known.
- Getting better insights in heterogeneous chemistry, including deposition reactions themselves.
- Developing models for new variations of CVI.

References

Adjerid, S., Flaherty, J.E., Hillig, W., Hudson, J., Shephard, M.S., 1995. Modeling and the adaptive solution of reactive vapor infiltration problems. Model. Simul. Mater. Sci. Eng. 3 (6), 737–752.

Bensoussan, J., Lions, J.-L., Papanicolaou, G., 1978. Asymptotic Analysis for Periodic Structure. North-Holland, Amsterdam.

Benzinger, W., Hüttinger, K.J., 1996. Chemical vapour infiltration of pyrocarbon: I. Some kinetic considerations. Carbon 34 (12), 1465–1471.

Benzinger, W., Hüttinger, K.J., 1998. Chemical vapor infiltration of pyrocarbon—II. The influence of increasing methane partial pressure at constant total pressure on infiltration rate and degree of pore filling. Carbon 36 (7/8), 1033–1042.

Benzinger, W., Hüttinger, K.J., 1999b. Chemistry and kinetics of chemical vapor infiltration of pyrocarbon—IV. Investigation of methane/hydrogen mixtures. Carbon 37 (6), 931–940.

Benzinger, W., Hüttinger, K.J., 1999c. Chemistry and kinetics of chemical vapor infiltration of pyrocarbon—V. Infiltration of carbon fiber felt. Carbon 37 (6), 941–946.

Bertrand, S., Lavaud, J.-F., El-Hadi, R., Vignoles, G.L., Pailler, R., 1998. The thermal-gradient pulsed-power flow CVI process: a new chemical vapor infiltration technique for the densification of fiber preforms. J. Eur. Ceram. Soc. 18 (7), 857–870.

Besmann, T.M., Sheldon, B.W., Kaster, M.D., 1990. Temperature and concentration dependence of SiC deposition on Nicalon fibers. Surf. Coat. Technol. 43–44 (1), 167–175.

Besmann, T.M., McLaughlin, J.C., Starr, T.L., 1994. Scale up and modeling of forced CVI. In: Logan, K. (Ed.), In: Proceedings of the 18th Annual Conference on Composites and Advanced Materials—B, vol. 15. The American Ceramic Society, Westerville, OH, pp. 897–907.

Besmann, T.M., Matlin, W.M., Starr, T.L., Curtain, W.A., 1995. Forced chemical vapor infiltration of tubular geometries: modeling, design and scale-up. In: Lowden, R.A., Ferber, M.K., Hellmann, J.R., Chawla, K.K., DiPietro, S.G. (Eds.), Ceramic Matrix Composites–Advanced High-Temperature Structural Materials, vol. 365 of Mater. Res. Soc. Symp. Proc. Materials Research Society, Pittsburgh, PA, pp. 317–321.

Bourgeat, A., Quintard, M., Whitaker, S., 1988. Comparison between homogenization theory and volume averaging method with closure problem (in French). C. R. Acad. Sci. II 306 (7), 463–466.

Brennfleck, K., Fitzer, E., Schoch, G., Dietrich, M., 1984. CVD of SiC-interlayers and their interaction with carbon fibers and with multi-layered NbN-coatings. In: Robinson, M., van den Brekel, C.H.J., Cullen, G.W., Blocher, J.M., Ray-Choudhury, P. (Eds.), Proceedings of the 9th International Conference CVD (I-CVD 9), vol. PV 84-6 of ECS Conf. Proc. The Electrochemical Society, Pennington, NJ, pp. 649–662.

Burganos, V.N., Sotirchos, S.V., 1989. Knudsen diffusion in parallel, multidimensional, or randomly oriented pore structures. Chem. Eng. Sci. 44, 2451–2462.

Carolan, M.F., Michaels, J.N, 1987. Chemical vapor deposition of Yttria stabilized zirconia on porous supports. Solid State Ionics 25 (2/3), 207–216.

Cavalier, J.C., Berdoyes, I., Bouillon, E., 2006. Composites in aerospace industry. Adv. Sci. Technol. 50, 153–162.

Chandrasekhar, S., 1943. Stochastic problems in physics and astronomy. Rev. Mod. Phys. 15 (1), 1–89.

Chang, H.C., Morse, T.F., Sheldon, B.W., 1997. Minimizing infiltration times during isothermal chemical vapor infiltration with methyltrichlorosilane. J. Am. Ceram. Soc. 80 (7), 1805–1811.

Chang, H.C., Gottlieb, D., Marion, M., Sheldon, B.W., 1998. Mathematical analysis and optimization of infiltration processes. J. Sci. Comput. 13 (3), 303–321.

Christin, F., 2005. A global approach to fiber *n*D architectures and self-sealing matrices: from research to production. Int. J. Appl. Ceram. Technol. 2, 97–104.

Chung, G.-Y., McCoy, B.J., 1991. Modeling of chemical vapor infiltration for ceramic composites reinforced with layered, woven fabrics. J. Am. Ceram. Soc. 74 (4), 746–751.

Chung, G.-Y., McCoy, B.J., Smith, J.M., Cagliostro, D.E., Carswell, M., 1991. Chemical vapor infiltration—modelling solid matrix deposition in ceramic-matrix composites. Chem. Eng. Sci. 46 (3), 723–734.

Chung, G.-Y., McCoy, B.J., Smith, J.M., Cagliostro, D.E., 1992. Chemical vapor infiltration: modelling solid matrix deposition for ceramic composites reinforced with layered woven fabrics. Chem. Eng. Sci. 47 (2), 311–323.

Chung, G.-Y., McCoy, B.J., Smith, J.M., Cagliostro, D.E., 1993. Chemical vapor infiltration: dispersed and graded depositions for ceramic composites. AlChE J. 39 (11), 1834–1846.

Coindreau, O., Vignoles, G.L., 2004. Computing structural and transport properties of C/C composites from 3D tomographic images. In: Martins, R., Dias, C., Fortunato, E., Ferreira, I., Godinho, H., Monteiro, R. (Eds.), Advanced Materials Forum II, vol. 455–456 of Mater. Sci. Forum, Zurich. Trans. Tech. Publications, pp. 751–754.

Coindreau, O., Vignoles, G.L., 2005. Assessment of geometrical and transport properties of a fibrous C/C composite preform as digitized by X-ray computed micro-tomography. Part I: image acquisition and geometrical properties. J. Mater. Res. 20 (9), 2328–2339.

Coindreau, O., Vignoles, G.L., Goyhénèche, J.-M., 2005. Multiscale X-ray CMT of C/C composites: a tool forproperties assessment. In: Bansal, N.P., Singh, J.P., Kriven, W.M. (Eds.), Multiscale X-ray CMT of C/C Composites: A Tool for Properties Assessment, vol. 175 of Ceram. Trans. The American Ceramic Society, Westerville, OH, pp. 77–84.

Coindreau, O., Mulat, C., Germain, C., Lachaud, J., Vignoles, G.L., 2011. Benefits of X-ray CMT for the modelling of C/C composites. Adv. Eng. Mater. 13 (3), 178–185.

Couégnat, G., Ros, W., Haurat, T., Germain, C., Martin, E., Vignoles, G.L., 2012. An integrated virtual material approach for ceramic matrix composites. In: Waltraud, M., Kriven, A.L., Gyekenyesi, Y.Z., Westin, G., Wang, J. (Eds.), Developments in Strategic Materials and Computational Design III, vol. 33 of Ceram. Eng. Sci. Proc. The American Ceramic Society, Wiley, New York, pp. 83–91.

Currier, R.P., 1990. Overlap model for chemical vapor infiltration of fibrous yarns. J. Am. Ceram. Soc. 73 (8), 2274–2280.

Currier, R.P., Valone, S.M., 1990. Time-dependent solution to the Tai-Chou chemical vapor infiltration model. J. Am. Ceram. Soc. 73 (6), 1758–1759.

Currier, R.P., Devlin, D.J., Morzinski, J., 1996. Dynamics of chemical vapor infiltration in carbon fiber bundles. Adv. Mater. 27 (4), 13–24.

Dekker, J.P., Moene, R., Schoonman, J., 1996. The influence of surface kinetics in modelling chemical vapour infiltration. J. Mater. Sci. 31 (11), 3021–3033.

Descamps, C., Vignoles, G.L., Féron, O., Langlais, F., Lavenac, J., 2001a. Correlation between homogeneous propane pyrolysis and pyrocarbon deposition. J. Electrochem. Soc. 148 (10), C695–C708.

Descamps, C., Vignoles, G., Féron, O., Lavenac, J., Langlais, F., 2001b. Kinetic modelling of gas-phase decomposition of propane: correlation with pyrocarbon deposition. J. Phys. IV 11 (PR3), 101–108.

Ditkowski, A., Gottlieb, D., Sheldon, B.W., 2000. Optimization of chemical vapor infiltration with simultaneous powder formation. J. Mater. Res. 15 (12), 2695–2705.

Einstein, A., 1956. Investigations on the Theory of the Brownian Movement (Trans. by Cowper A.D.). Dover Edition, Berlin.

Ekhlakov, A., Dimitrov, S., Langhoff, T.-A., Schnack, E., 2008. Phase-field model for deposition of pyrolytic carbon. Comm. Numer. Meth. Eng 24 (12), 2139–2154.

Evans, D., Evans, J.W., 1993. A mathematical model for CVI with microwave heating and external cooling. J. Am. Ceram. Soc. 76 (8), 1924–1932.

Fédou, R., Langlais, F., Naslain, R., 1993. A model for the isothermal isobaric CVI in a straight cylindrical pore. Application to the CVI of SiC. J. Mater. Synth. Process. 1 (2), 61–74.
Féron, O., Langlais, F., Naslain, R., Thébault, J., 1999. On kinetic and microstructural transitions in the CVD of pyrocarbon from propane. Carbon 37 (9), 1343–1353.
Fitzer, E., Fritz, W., Schoch, G., 1992. Modelling of the chemical vapor impregnation of porous (carbon) substrates with SiC. High Temp. High Press. 24 (3), 343–354.
Golecki, I., 1997. Rapid vapor-phase densification of refractory composites. Mater. Sci. Eng. Rep. R20, 37–124.
Golecki, I., Morris, R.C., Narasimhan, D., Clements, N., 1996. Carbon-carbon composites inductively-heated and rapidly densified by thermal-gradient chemical vapor infiltration: density distributions and densification mechanism. In: Logan, K.V., Munir, Z.A., Spriggs, R.M. (Eds.), Advanced Synthesis and Processing of Composites and Advanced Ceramics II, vol. 79 of Ceram. Trans. The American Ceramic Society, Westerville, OH, pp. 135–142.
Goodwin, D.G., 2003. An open-source, extensible software suite for CVD process simulation. In: Allendorf, M., Maury, F., Teyssandier, F. (Eds.), Chemical Vapor Deposition XVI and EuroCVD 14, vol. 2003-08 of ECS Proc. The Electrochemical Society, Pennington, NJ, pp. 155–162.
Goujard, S., Charvet, J.-L., Leluan, J.-L., Abbé, F., Lamazouade, G., 1995. Matériau composite protégé contrel'oxydation par une matrice autocicatrisante et son procédé de fabrication, French Patent No. 9503606.
Griffiths, S.K., Nilson, R.H., 1998. Optimum conditions for composites fiber coating by chemical vapor deposition. J. Electrochem. Soc. 145 (4), 1263–1272.
Grujicic, M., 1994. An analysis of the isothermal isobaric chemical vapor infiltration of TiB_2. Calphad 18 (1), 81–88.
Guan, K., Cheng, L., Zeng, Q., Feng, Z.Q., Zhang, L., Li, H., Li, K., 2011. Modeling of pore structure evolution within the fiber bundle during chemical vapor infiltration process. Chem. Eng. Sci. 66 (23), 5852–5861.
Guan, K., Cheng, L., Zeng, Q., Zhang, L., Deng, J., Li, K., Li, H., 2013. Modeling of pore structure evolution between bundles of plain woven fabrics during chemical vapor infiltration process: the influence of preform geometry. J. Am. Ceram. Soc. 96 (1), 51–61.
Gupta, D., Evans, J.W., 1991. A mathematical model for CVI with microwave heating and external cooling. J. Mater. Res. 6 (4), 810–818.
Hashin, Z., Shtrikman, S., 1962. A variational approach to the theory of the effective magnetic permeability of multiphase materials. J. Appl. Phys. 33 (10), 3125–3131.
Hillig, W.B., Adjerid, S., Flaherty, J.E., Hudson, J.B., 1996. The effect of combined diffusion and kinetic transport barriers on multi-phase solid state reactions with a vapour reactant. J. Mater. Sci. 31 (22), 5865–5871.
Hou, X.-H., Li, H.-J., Chen, Y.-X., Li, K.-Z., 1999. Modeling of chemical vapor infiltration process for fabrication of carbon-carbon composites by finite difference methods. Carbon 37 (4), 669–677.
Hua, Y.-F., Zhang, L.-T., Cheng, L.-F., Li, Z.-X., Du, J.-H., 2009. A two-process model for study of the effect of fiber preform structure on isothermal chemical vapor infiltration of silicon carbide matrix composites. Comput. Mater. Sci. 46 (1), 133–141.
Ibrahim, J., Paolucci, S., 2011. Transient solution of chemical vapor infiltration/deposition in a reactors. Carbon 49 (3), 915–930.
Jin, S., Wang, X.-L., 2003. Robust numerical simulation of porosity evolution in chemical vapor infiltration III: three space dimensions. J. Comput. Phys. 186 (2), 582–595.

Johnson, D.L., Koplik, J., Schwartz, L.M., 1986. New pore-size parameter characterizing transport in porous media. Phys. Rev. Lett. 57 (20), 2564–2567.
Jones Jr., A.D., 2006. Profile of an unsuccessful process and the criteria for a successful process for the chemical vapor infiltration process. J. Appl. Math. Model. 30 (3), 293–306.
Jones Jr., A.D., 2007. Analysis of the chemical vapor infiltration process computational experiments. Comput. Math. Appl. 54 (9/10), 1213–1217.
Jones, M., Starr, T.L., 1995. Enhancements to the Georgia CVI process model for ceramic matrix composites. In: Pfendt, G.N. (Ed.), Enhancements to the Georgia CVI Process Model for Ceramic Matrix Composites, vol. 16 of Ceram. Eng. Sci. Proc. The American Ceramic Society, Westerville, OH, pp. 829–836.
Kawase, M., Ikuta, Y., Tago, T., Masuda, T., Hashimoto, K., 1994. Modeling of a thermal-gradient chemical vapor infiltration process for production of silicon carbide whisker/alumina composite. Chem. Eng. Sci. 49, 4861–4870.
Kim, I.C., Torquato, S., 1990. Determination of the effective conductivity of heterogeneous media by Brownian motion simulation. J. Appl. Phys. 68 (8), 3892–3903.
Kim, H., Chung, G., Koo, H., Baek, W., 2004. Effects of process parameters for the preparation of C/SiC composites in the F-chemical vapor infiltration reactor. Korean J. Chem. Eng. 21 (5), 929–934.
King, M.K., 1994. Modeling study of effects of temperature profiling on CVI processing of woven graphite preforms with dimethyldichlorosilane. J. Mater. Res. 9, 2174–2189.
Kinney, J.H., Breunig, T.M., Starr, T.L., Haupt, D., Nichols, M.C., Stock, S.R., Butts, M.D., Saroyan, R.A., 1993. X-ray tomographic study of chemical vapor infiltration processing of ceramic composites. Science 260 (5109), 789–792.
Kulik, V., Kulik, A., Ramm, M., Makarov, Y., 2004. Modeling of SiC-matrix composite formation by isothermal chemical vapor infiltration. J. Crystal Growth 266 (1–3), 333–339.
Lacroix, R., Fournet, R., Ziegler-Devin, I., Marquaire, P.M., 2010. Kinetic modeling of surface reactions involved in CVI of pyrocarbon obtained by propane pyrolysis. Carbon 48 (1), 132–144.
Langhoff, T.-A., Schnack, E., 2003. Modelling chemical vapour infiltration of pyrolytic carbon. In: Wendyland, W.I., Efendiev, M. (Eds.), Analysis and Simulation of Multifield Problems, vol. 12 of Lecture Notes in Applied and Computational Mechanics. International Conference on Multifield Problems, University of Stuttgart, Stuttgart, Germany, April 8–10, 2002, pp. 149-154.
Langhoff, T.A., Schnack, E., 2008. Modelling chemical vapour infiltration of pyrolytic carbon as moving boundary problem. Chem. Eng. Sci. 63 (15), 3948–3959.
Langlais, F., 2000. Chemical vapor infiltration processing of ceramic matrix composites. In: Zweben, A., Kelly, C. (Eds.), Comprehensive Composite Materials, vol. 4. Pergamon, Oxford, pp. 611–644 (Chapter 20).
Lavenac, J., Langlais, F., Féron, O., Naslain, R., 2001a. Microstructure of the pyrocarbon matrix in carbon/carbon composites. Compos. Sci. Technol. 61 (3), 339–345.
Lavenac, J., Langlais, F., Bourrat, X., Naslain, R., 2001b. Deposition process of laminar pyrocarbon from propane. In: Davazoglu, D., Vahlas, C. (Eds.), Euro-CVD 13 Proceedings, vol. 11 of J. Phys. IV France, Les Ulis, France. EDP Sciences, pp. Pr3-1013–Pr3-1021.
Lee, S.B., Stock, S.R., Butts, M.D., Starr, T.L., Breunig, T.M., Kinney, J.H., 1998. Pore geometry in woven fiber structures: 0°/90° plain-weave cloth layup preform. J. Mater. Res. 13 (5), 1209–1217.
Le Poche, H., Bourrat, X., Dourges, M.-A., Vignoles, G.L., Langlais, F., 2005. Influence of the gas-phase maturation on the CVD/CVI process and the micro-texture of laminar pyrocarbon from propane. In: Singh, M., Kerans, R.J., Lara-Curzio, E., Naslain, R. (Eds.), High-

Temperature Ceramic Matrix Composites, vol. 5. The American Ceramic Society, Wiley, New York, pp. 81–86.
Leutard, D., Vignoles, G.L., Lamouroux, F., Bernard, B., 2002. Monitoring density and temperature in C/C composites elaborated by CVI with radio-frequency heating. J. Mater. Synth. Proc. 9 (5), 259–273.
Lewis, J.S., Lackey, W.J., Vaidyaraman, S., 1997. Model for prediction of microstructure for carbon/carbon composites prepared by forced-flow-thermal gradient CVI. Carbon 35 (1), 103–112.
Li, A.J., Deutschmann, O., 2007. Transient modeling of chemical vapor infiltration of methane using multi-step reaction and deposition models. Chem. Eng. Sci. 62 (18–20), 4976–4982.
Li, K.-Z., Li, H.-J., Jiang, K.-Y., Hou, X.-H., 2000. Numerical simulation of isothermal chemical vapor infiltration process in fabrication of carbon-carbon composites by finite element method. Sci. China E 43 (1), 77–85.
Li, A.-J., Li, H.-J., Li, K.-Z., Gu, Z.-B., 2003. Modeling of CVI process in fabrication of carbon/carbon composites by an artificial neural network. Sci. China E 46 (2), 173–181.
Li, A.-J., Li, H.-J., Li, K.-Z., Gu, Z.-B., 2004. Applications of neural networks and genetic algorithms to CVI processes in carbon/carbon composites. Acta Mater. 52 (2), 299–305.
Li, H.-J., Li, A.-J., Li, K.-Z., Bai, R.-C., 2005. Numerical simulation of chemical vapor infiltration of propylene into C/C composites with reduced multi-step kinetic models. Carbon 43 (14), 2937–2950.
Li, A.-J., Norinaga, K., Zhang, W., Deutschmann, O., 2008. Modelling and simulation of materials synthesis: chemical vapor deposition and infiltration of pyrolytic carbon. Compos. Sci. Technol. 68 (5), 1097–1104.
Lieberman, M.L., Pierson, H.O., 1974. Effect of gas phase conditions on resultant matrix pyrocarbon in carbon/carbon composites. Carbon 12 (3), 233–241.
Lines, J.F., Vignoles, G.L., Goyhénèche, J.M., Puiggali, J.R., 2005. Thermal modelling of a carbon/carbon composite material fabrication. In: Denis, S. (Ed.), Proceedings of the International Conference on Thermal Process Modelling and Computer Simulation 2003, vol. 120 of J. Phys. IV France. EDP Sciences, Les Ulis, France, pp. 291–297.
Lu, G.Q., 1993. Modelling the densification of porous structures in CVI ceramic composites processing. J. Mater. Proc. Technol. 37 (1–4), 487–498.
McAllister, P., Wolf, E.E., 1993. Simulation of a multiple substrate reactor for chemical vapor infiltration of pyrolytic carbon within carbon-carbon composites. AIChE J. 39 (7), 1196–1209.
Melkote, R.R., Jensen, K.F., 1989. Gas diffusion in random-fiber substrates. AIChE J. 35 (12), 1942–1956.
Melkote, R.R., Jensen, K.F., 1990. A model for chemical vapor infiltration of fibrous substrates. In: Besmann, T.M., Gallois, B.M. (Eds.), Chemical Vapor Deposition of Refractory Metals and Ceramics, vol. 168 of Mater. Res. Soc. Symp. Proc. Materials Research Society, Pittsburgh, PA, pp. 67–72.
Melkote, R.R., Jensen, K.F., 1992. Computation of transition and molecular diffusivities in fibrous media. AIChE J. 38 (1), 56–61.
Middleman, S., 1989. The interaction of chemical kinetics and diffusion in the dynamics of chemical vapor infiltration. J. Mater. Res. 4 (6), 1515–1524.
Midha, V., Economou, D.J., 1997. A two-dimensional model of chemical vapor infiltration with radio frequency heating. J. Electrochem. Soc. 144 (11), 4062–4071.
Midha, V., Economou, D.J., 1998. A two-dimensional model of chemical vapor infiltration with radio frequency heating. II. Strategies to achieve complete densification. J. Electrochem. Soc. 145 (10), 4062–4071.

Minkina, V.G., 1997. Chemical vapor deposition in a porous body. Theor. Found. Chem. Eng. 31 (3), 248–252.

Morell, J.I., Economou, D.J., Amundson, N.R., 1992a. A mathematical model for chemical vapor infiltration with volume heating. J. Electrochem. Soc. 139 (1), 328–336.

Morell, J.I., Economou, D.J., Amundson, N.R., 1992b. Pulsed-power volume-heating chemical vapor infiltration. J. Mater. Res. 7 (9), 2447–2457.

Morell, J.I., Economou, D.J., Amundson, N.R., 1993. Chemical vapor infiltration of SiC with microwave heating. J. Mater. Res. 8 (5), 1057–1067.

Mulat, C., 2008. Detection Characterization of 3D Objects and Morphological Evolution Simulation Applied to the Infiltrability of Fibrous Preforms. Ph.D. Thesis. University of Bordeaux.

Nadeau, N., Vignoles, G.L., Brauner, C.M., 2006. Analytical and numerical study of the densification of carbon/carbon composites by a film-boiling chemical vapor infiltration process. Chem. Eng. Sci. 61 (22), 7509–7527.

Naslain, R., Langlais, F., 1986. CVD-processing of ceramic-ceramic composite materials. In: Tressler, R.E., Messing, G.E., Pantano, C.G., Newnham, R.E. (Eds.), Tailoring Multiphase and Composite Ceramics, vol. 20 of Mater. Sci. Res. Kluwer Academic Publisher, Dordrecht, The Netherlands, pp. 145–164.

Naslain, R., Langlais, F., Vignoles, G.L., Pailler, R., 2006. The CVI-process: state of the art and perspective. In: Wereszczak, A., Lara-Curzio, E., Tandon, R. (Eds.), Mechanical Properties and Performance of Engineering Ceramics II, vol. 27 of Ceram. Eng. Sci. Process. The American Ceramic Society, Wiley, New York, pp. 373–386.

Norinaga, K., Deutschmann, O., 2007. Detailed kinetic modeling of gas phase reactions in chemical vapor deposition of carbon from light hydrocarbons. Ind. Eng. Chem. Res. 46 (11), 3547–3557.

Oberlin, A., 1984. Carbonization and graphitization. Carbon 22 (6), 521–541.

Ofori, J.Y., Sotirchos, S.V., 1996a. Optimal pressures and temperatures for isobaric isothermal CVI. AIChE J. 42 (10), 2828–2840.

Ofori, J.Y., Sotirchos, S.V., 1996b. Structural model effects on the predictions of CVI models. J. Electrochem. Soc. 143 (6), 1962–1973.

Ofori, J.Y., Sotirchos, S.V., 1996c. Dynamic convection-driven thermal gradient chemical vapor infiltration. J. Mater. Res. 11 (10), 2541–2555.

Ofori, J.Y., Sotirchos, S.V., 1997a. Multidimensional modelling of chemical vapor infiltration: application to isobaric CVI. Ind. Eng. Chem. Res. 36 (2), 357–367.

Ofori, J.Y., Sotirchos, S.V., 1997b. Investigation of the potential of forced-flow chemical vapor infiltration. J. Electrochem. Soc. 144 (1), 274–289.

Ofori, J.Y., Sotirchos, S.V., 1997c. Multidimensional transport effects on forced-flow chemical-vapor infiltration. Ind. Eng. Chem. Res. 36 (5), 1921–1931.

Patibandla, N., Hillig, W.B., 1993. Processing of molybdenum disilicide using a new reactive vapor infiltration technique. J. Am. Ceram. Soc. 76 (6), 1630–1634.

Pierson, H.O. (Ed.), 1988. Handbook of Thin-Film Deposition Processes and Techniques, first ed. Materials Science and Process Technology Series, Noyes, Park Ridge, NJ, USA.

Probst, K.J., Besmann, T.M., Stinton, D.P., Lowden, R.A., Anderson, T.J., Starr, T.L., 1999. Recent advances in forced-flow, thermal-gradient CVI for refractory composites. Surf. Coat. Technol. 120–121, 250–258.

Reuge, N., Vignoles, G.L., 2005. Modeling of isobaric-isothermal chemical vapor infiltration: effects of reactor control parameters on a densification. J. Mater. Process. Technol. 166 (1), 15–29.

Reuge, N., Vignoles, G.L., Le Poche, H., Langlais, F., 2002. Modelling of pyrocarbon chemical vapor infiltration. In: Vicenzini, P., Lami, A. (Eds.), Proceedings of the CIMTEC/3rd

Forum on New Materials, vol. 1: Computational Modelling and Simulation of Materials II, vol. 36 of Adv. Sci. Technol. Techna, Faenza, Italy, pp. 259–266.
Reznik, B., Hüttinger, K.J., 2002. On the terminology for pyrolytic carbons. Carbon 40 (4), 621–624.
Roman, Y., 1994. Forced Flow Chemical Vapour Infiltration. Ph.D. Thesis. T.U. Eindhoven.
Roman, Y.G., Kotte, J.F.A.K., de Croon, M.H.J.M., 1995. Analysis of the isothermal forced flow chemical vapour infiltration process. Part I: theoretical aspects. J. Eur. Ceram. Soc. 15 (9), 875–886.
Ros, W., Vignoles, G.L., Germain, C., Supiot, P., Kokkoris, G., 2011. Simulation of chemical vapor infiltration and deposition based on 3D images: a local scale approach. Chem. Vap. Deposition 17 (10–12), 312–320.
Rossignol, J.Y., Langlais, F., Naslain, R., 1984. A tentative modelization of titanium carbide CVI within the pore network of two-dimensional carbon–carbon composites preforms. In: Robinson, M., van den Brekel, C.H.J., Cullen, G.W., Blocher, J.M., Ray-Choudhury, P. (Eds.), Proceedings of the 9th International Conference on CVD (I-CVD 9), vol. PV 84-6, ECS Conf. Proc. The Electrochemical Society, Pennington, NJ, pp. 594–614.
Rovillain, D., Trinquecoste, M., Bruneton, E., Derré, A., David, P., Delhaès, P., 2001. Film-boiling chemical vapor infiltration. An experimental study on carbon/carbon composites. Carbon 39 (9), 1355–1365.
Sanchez-Palencia, E., 1980. Non-Homogeneous Media and Vibration Theory, vol. 127 of Lecture Notes in Physics. Springer-Verlag, New York.
Schnack, E., Wang, F.W., Li, A.J., 2010. Phase-field model for the chemical vapor infiltration of silicon carbide. J. Electrochem. Soc. 157 (7), D377–D386.
Schoch, G., Fritz, W., Fitzer, E., 1991. Ceramic/ceramic composite materials. Modelling of CVI process. Contract MAIE/0018/C, EURAM.
Skamser, D.J., Bentz, D.P., Coverdale, R.T., Spotz, M.S., Martys, N., Jennings, H., Johnson, D.L., 1994. Calculation of the thermal conductivity and gas permeability in a uniaxial bundle of fibers. J. Am. Ceram. Soc. 77 (10), 2669–2680.
Skamser, D.J., Jennings, H.M., Johnson, D.L., 1997. Model of chemical vapor infiltration using temperature gradients. J. Mater. Res. 12 (3), 724–737.
Sotirchos, S.V., 1991. Dynamic modelling of chemical vapor infiltration. AIChE J. 37 (9), 1365–1382.
Sotirchos, S.V., Tomadakis, M.M., 1990. Modeling transport, reaction and pore structure evolution during densification of cellular or fibrous structure. In: Besmann, T.M., Gallois, B.M. (Eds.), Chemical Vapor Deposition of Refractory Metals and Ceramics, vol. 168 of Mater. Res. Soc. Symp. Proc. Materials Research Society, Pittsburgh, PA, pp. 73–78.
Starr, T.L., 1988. Modeling of forced flow/thermal gradient CVI. In: Bradley, R.A., Clark, D.E., Larsen, D.S., Stiegler, J.Q. (Eds.), In: Proceedings of the International Conference on Whisker and Fiber-Thoughened Ceramics. ASM, Metals Park, OH, p. 243.
Starr, T.L., 1995. Gas transport model for CVI. J. Mater. Res. 10 (9), 2360–2366.
Starr, T., Smith, A., 1990. 3D modeling of forced flow thermal gradient CVI for ceramic composite fabrication. In: Besmann, T.M., Gallois, B.M. (Eds.), Chemical Vapor Deposition of Refractory Metals and Ceramics, vol. 168 of Mater. Res. Soc. Symp. Proc. Materials Research Society, Pittsburgh, PA, pp. 55–60.
Starr, T.L., Smith, A.W., 1992a. Advances in modeling of the forced chemical vapor infiltration process. In: Palmer, K. (Ed.), Structural Carbons: Proceedings of the 8th Annual Conference on Materials Technology. South Illinois University at Carbondale Materials Technology Center, Carbondale, IL, USA, pp. 219–233.

Starr, T.L., Smith, A.W., 1992b. Modeling of chemical vapor infiltration for ceramic and carbon matrix composites. In: Besmann, T.M. (Ed.), Chemical Vapor Deposition of Refractory Metals and Ceramics II, vol. 250 of Mat. Res. Soc. Symp. Proc. Materials Research Society, Pittsburgh, PA, pp. 207–214.

Starr, T.L., Smith, A.W., Vinyard, G.F., 1991. Model-assisted control of CVI for ceramic fabrication. In: Wachtman, J.B. (Ed.), Proceedings of the 15th Annual Conference on Composites and Advanced Ceramic Materials, vol. 12 of Ceram. Eng. Sci. Proc. The American Ceramic Society, Westerville, OH, pp. 2017–2028.

Starr, T.L., Smith, A.W., Besmann, T.M., McLaughlin, J., 1993. Modeling of chemical vapor infiltration for composite fabrication. In: Naslain, R., Lamon, J., Doumeingts, D. (Eds.), Proceedings of the International Conference on High-Temperature Ceramic-Matrix Composites (HT-CMC). Woodhead Publishing Ltd, Cambridge, pp. 231–240.

Stinton, D.P., Besmann, T.M., Matlin, W.M., Starr, T.L., Curtain, W.A., 1995. Forced chemical vapor infiltration of tubular geometries: modeling, design and scale-up. In: Lowden, R.A., Ferber, M.K., Hellmann, J.R., Chawla, K.K., DiPietro, S.G. (Eds.), Ceramic Matrix Composites–Advanced High-Temperature Structural Materials, vol. 365 of Mater. Res. Soc. Symp. Proc. Materials Research Society, Pittsburgh, PA, pp. 317–324.

Tai, N.H., Chou, T.W., 1988. Theoretical analysis of chemical vapor infiltration in ceramic/ceramic composites. In: Lemkey, F.D., Fishman, S.G., Evans, A.G., Strife, J.R. (Eds.), High Temperature/High Performance Composites, vol. 120 of Mater. Res. Soc. Symp. Proc. Materials Research Society, Pittsburgh, PA, p. 185.

Tai, N.H., Chou, T.W., 1989. Analytical modeling of chemical vapor infiltration of ceramic composites. J. Am. Ceram. Soc. 72 (3), 414–420.

Tai, N.H., Chou, T.W., 1990a. Theoretical modeling of the chemical vapor infiltration process for Forfming highly densified ceramic/ceramic composites. In: Bhagat, A.B., Clauer, A.H., Kumar, P., Ritter, A.M. (Eds.), Proceedings of the 119th TMS Annual Meeting—Metal and Ceramic Matrix Composites: Processing, Modeling & Mechanical Behavior. The Metallurgical Society, Warrendale, PA, USA, pp. 303–309.

Tai, N.H., Chou, T.W., 1990b. Modeling of an improved CVI process for ceramic composites fabrication. J. Am. Ceram. Soc. 73 (6), 1489–1498.

Tai, N.H., Chou, T.W., Ma, C.C.M., 1994. Effects of deposition mechanisms in the modeling of forced flow/temperature gradient chemical vapor infiltration. J. Am. Ceram. Soc. 77 (3), 849–851.

Thiele, E.W., 1939. Relation between catalytic activity and size of particles. Ind. Eng. Chem. 31 (7), 916–920.

Tilley, B.S., Kriegsmann, G.A., 2001. Microwave-enhanced chemical vapor infiltration: a sharp interface model. J. Eng. Mech. 41 (1), 33–54.

Tomadakis, M.M., Robertson, T.J., 2005. Viscous permeability of random fiber structures: comparison of electrical and diffusional estimates with experimental and analytical results. J. Compos. Mater. 39 (2), 163–188.

Tomadakis, M.M., Sotirchos, S.V., 1991a. Effective Knudsen diffusivities in structures of randomly overlapping fibers. AIChE J. 37 (1), 74–86.

Tomadakis, M.M., Sotirchos, S.V., 1991b. Knudsen diffusivities and properties of structures of unidirectional fibers. AIChE J. 37 (8), 1175–1186.

Tomadakis, M.M., Sotirchos, S.V., Gallois, B.M., Warren, J.W., 1992. Effects of fiber orientation and overlapping on Knudsen, transition, and ordinary regime diffusion in fibrous structures. In: Besmann, T.M. (Ed.), Chemical Vapor Deposition of Refractory Metals and Ceramics II, vol. 250 of Mater. Res. Soc. Symp. Proc. Materials Research Society, Pittsburgh, PA, pp. 221–226.

Tomadakis, M.M., Sotirchos, S.V., 1993a. Transport properties of random arrays of freely overlapping cylinders with various orientation distributions. J. Chem. Phys. 98 (1), 616–626.

Tomadakis, M.M., Sotirchos, S.V., 1993b. Ordinary, transition and Knudsen regime diffusion in random capillary structures. Chem. Eng. Sci. 48 (19), 3323–3333.

Tomadakis, M.M., Sotirchos, S.V., 1993c. Ordinary and transition regime diffusion in random fiber structures. AIChE J. 39 (3), 397–412.

Tomadakis, M.M., Sotirchos, S.V., 1996. Transport through random arrays of conductive cylinders dispersed in a conductive matrix. J. Chem. Phys. 104 (17), 6893–6900.

Torquato, S., 2002. Random Heterogeneous Materials. Springer-Verlag, New York.

Torquato, S., Kim, I.C., 1989. Efficient simulation technique to compute effective properties of heterogeneous media. Appl. Phys. Lett. 55 (18), 1847–1849.

Transvalidou, F., Sotirchos, S.V., 1996. Effective diffusion coefficients in square arrays of filament bundles. AIChE J. 42 (9), 2426–2438.

Tsai, C.Y., Desu, S.B., 1991. Contribution of gas-phase reactions to the deposition of SiC by a forced-flow chemical vapor infiltration process. In: Besmann, T.M., Gallois, B.M., Warren, J.W. (Eds.), Chemical Vapor Deposition of Refractory Metals and Ceramics II, vol. 250 of Mater. Res. Soc. Symp. Proc. Materials Research Society, Pittsburgh, PA, pp. 227–232.

Vaidyaraman, S., Lackey, W.J., Freeman, G.B., Agrawal, P.K., Langman, M.D., 1995. Fabrication of carbon–carbon composites by forced flow-thermal gradient chemical vapor infiltration. J. Mater. Res. 10 (6), 1469–1477.

Vaidyaraman, S., Lackey, W.J., Agrawal, P.K., Starr, T.L., 1996. 1-D model for forced-flow-thermal gradient chemical vapor infiltration process for carbon/carbon composites. Carbon 34 (9), 1123–1133.

van den Brekel, C.H.J., Fonville, R.M.M., van der Straten, P.J.M., Verspui, G., 1981. CVD of Ni, TiN and TiC on complex shapes. In: Blocher Jr., J.M., Vuillard, G.E., Wahl, G. (Eds.),. Proceedings of the International Conference on CVD, vol. PV 81-7 of ECS Conf. Proc. The Electrochemical Society Inc., Pennington, NJ, USA, pp. 142–156.

Vignoles, G.L., 1995. Modelling binary, Knudsen and transition regime diffusion in side complex porous media. J. Phys. IV 5 (C5), 159–166.

Vignoles, G.L., 2001. Image segmentation for hard X-ray phase contrast images of C/C composites. Carbon 39 (2), 167–173.

Vignoles, G.L., 2006. Modelling of the CVI processes. In: Vincenzini, P., Singh, M. (Eds.), Advanced Inorganic Fibrous Composites V, vol. 50 of Adv. Sci. Technol., pp. 97–106.

Vignoles, G.L., Descamps, C., Reuge, N., 2000. Interaction between a reactive preform and the surrounding gas-phase during CVI. J. Phys. IV 10 (P2), 9–17.

Vignoles, G.L., Langlais, F., Descamps, C., Mouchon, A., Le Poche, H., Reuge, N., Bertrand, N., 2004. CVD and CVI of pyrocarbon from various precursors. Surf. Coat. Technol. 188–189, 241–249.

Vignoles, G.L., Nadeau, N., Brauner, C.-M., Lines, J.-F., Puiggali, J.-R., 2005. The notion of densification front in CVI processing with temperature gradients. In: Zhu, D., Lara-Curzio, E., Kriven, W.M. (Eds.), Mechanical Properties and Performance of Engineering Ceramics and Composites, vol. 26 of Ceram. Eng. Sci. Proc. The American Ceramic Society, Westerville, OH, pp. 187–195.

Vignoles, G.L., Goyhénèche, J.M., Sébastian, P., Puiggali, J.R., Lines, J.F., Lachaud, J., Delhaès, P., Trinquecoste, M., 2006. The film-boiling densification process for C/C composite fabrication: from local scale to overall optimization. Chem. Eng. Sci. 61 (17), 5636–5653.

Vignoles, G.L., Coindreau, O., Ahmadi, A., Bernard, D., 2007a. Assessment of geometrical and transport properties of a fibrous C/C composite preform as digitized by X-ray computerized micro-tomography. Part II: heat and gas transport. J. Mater. Res. 22 (6), 1537–1550.

Vignoles, G.L., Coindreau, O., Ahmadi, A., Bernard, D., 2007b. Assessment of geometrical and transport properties of a fibrous C/C composite preform as digitized by X-ray computerized microtomography. Part II: heat and gas transport properties. J. Mater. Res. 22 (6), 1537–1550.

Vignoles, G.L., Duclous, R., Gaillard, S., 2007c. Analytical stability study of the densification front in carbon- or ceramic-matrix composites processing by TG-CVI. Chem. Eng. Sci. 62 (22), 6081–6089.

Vignoles, G.L., Gaborieau, C., Delettrez, S., Chollon, G., Langlais, F., 2008. Reinforced carbon foams prepared by chemical vapor infiltration: a process modeling approach. Surf. Coat. Technol. 203 (5–7), 510–515.

Vignoles, G.L., Germain, C., Coindreau, O., Mulat, C., Ros, W., 2009. Fibre-scale modelling of C/C processing by chemical vapour infiltration using X-ray CMT images and random walkers. In: Swihart, M.T., Barreca, D., Adomaitis, R.A., Wörkhoff, K. (Eds.), ICVD XVII and EuroCVD 17 Proceedings, vol. 25 of ECS Transactions. The Electrochemical Society, Pennington, NJ, pp. 1275–1284.

Vignoles, G.L., Germain, C., Mulat, C., Coindreau, O., Ros, W., 2010a. Modeling of infiltration of fiber preforms based on X-ray tomographic imaging. In: Vicenzini, P., Ferrar, M., Singh, M. (Eds.), 12th International Ceramics Congress Part J, vol. 71 of Adv. Sci. Technol. Trans Tech Publications, pp. 108–117.

Vignoles, G.L., Coindreau, O., Ros, W., Szelengowicz, I., Mulat, C., Germain, C., Donias, M., 2010b. Modelling chemical vapour infiltration in C/C composites: numerical tools based on μ-CT images. In: Krenkel, W., Lamon, J. (Eds.), HT-CMC7—7th International Conference on High-Temperature Ceramic-Matrix Composites, Bayreuth, Germany. AVISO Verlag-Gesellschaft, Berlin, pp. 598–606.

Vignoles, G., Szelengowicz, I., Ros, W., Mulat, C., Germain, C., 2010c. Isothermal chemical vapor infiltration modeling by random walks in CMT 3D images at two scales. In: Singh, D., Salem, J. (Eds.), Mechanical Properties and Performance of Engineering Ceramics and Composites, vol. 31 of Ceram. Eng. Sci. Proc. The American Ceramic Society, Wiley, Westerville, OH/New York, pp. 329–340.

Vignoles, G.L., Donias, M., Mulat, C., Germain, C., Delesse, J.F., 2011a. Simplified marching cubes: an efficient discretization scheme for simulations of deposition/ablation in complex media. Comput. Mater. Sci. 50 (3), 893–902.

Vignoles, G.L., Ros, W., Mulat, C., Coindreau, O., Germain, C., 2011b. Pearson random walk algorithms for fiber-scale modeling of chemical vapor infiltration. Comput. Mater. Sci. 50 (3), 1157–1168.

Vignoles, G.L., Ros, W., Szelengowicz, I., Germain, C., 2011c. A Brownian motion algorithm for tow-scale modeling of chemical vapor infiltration. Comput. Mater. Sci. 50 (6), 1871–1878.

Vignoles, G.L., Pailler, R., Teyssandier, F., 2012. The control of interphases in carbon and ceramic matrix composites. In: Halbig, M., Ohji, T., Singh, M., Mathur, S. (Eds.), Advanced Processing and Manufacturing Technologies for Structural and Multifunctional Materials VI, vol. 33 of Ceram. Eng. Sci. Proc. Wiley, New York, pp. 11–23.

Vignoles, G.L., Ros, W., Chollon, G., Langlais, F., Germain, C., 2013. Quantitative validation of a multi-scale model of pyrocarbon chemical vapor infiltration from propane. In: Ohji, T., Singh, M. (Eds.), Advanced Processing and Manufacturing Technologies

for Structural and Multifunctional Materials and Systems VI (APMT6), vol. 33 of Ceram. Eng. Sci. Proc. The American Ceramic Society, Wiley, New York, pp. 147–157.

Vignoles, G.L., Ros, W., Germain, C., 2014a. Numerical estimation of the infiltrability of woven CMC preforms. In: Kriven, W.M., Gyekenyesi, A.L., Zhou, Y.-C., Wang, J.-Y. (Eds.), Developments in Strategic Materials and Computational Design IV, vol. 34 of Ceram. Eng. Sci. Proc. The American Ceramic Society, Wiley, New York, pp. 267–271.

Vignoles, G.L., Chapoullié, C., Ros, W., Mulat, C., Couégnat, G., Germain, C., Da Costa, J.P., Cataldi, M., Descamps, C., 2014b. Contribution of image processing techniques to the simulation of chemical vapor infiltration of SiC in CMCs. In: Zhang, L., Jiang, D. (Eds.), Proceedings of the HT-CMC 8, vol. 248 of Ceram. Trans. The American Ceramic Society, Wiley, pp. 29–38.

Wang, F.W., Schnack, E., Zhu, Y.C., 2013. Discontinuous Galerkin solution of a phase-field model in isothermal chemical vapor infiltration of SiC. J. Eng. Math. 78 (1, SI), 261–274.

Wei, X., Cheng, L.F., Zhang, L.T., Xu, Y.D., Zeng, Q.F., 2006a. Numerical simulation for fabrication of C/SiC composites in isothermal CVI reactor. Comput. Mater. Sci. 38 (2), 245–255.

Wei, X., Cheng, L.F., Zhang, L.T., Xu, Y.D., Zeng, Y.D., 2006b. Numerical simulation of effect of methyltrichlorosilane flux on isothermal chemical vapor infiltration process of C/SiC composites. J. Am. Ceram. Soc. 89 (9), 2762–2768.

Wei, X., Cheng, L.F., Zhang, L.T., Xu, Y.D., Zeng, Q.F., 2007. Modeling the effects of reactor wall reaction on isothermal CVI process of C/SiC composites. Comput. Mater. Sci. 38 (4), 702–706.

Wei, X., Cheng, L.F., Zhang, L.T., Xu, Y.D., Pan, W., 2008. Numerical simulation of effects of reactor dimensions on isothermal CVI process of C/SiC composites. Comput. Mater. Sci. 44 (2), 670–677.

Whitaker, S., 1999. The Method of Volume Averaging. Kluwer Academic Publishers, New York.

Wiener, O., 1912. Die theorie des mischkörpers für dasfeld der stationären strömung. 1. Abhandlung: Diemittelwertsätze für kraft, polarisation und energie. Abhandlungen der Mathematisch-Physischen Klasse der Königlichen Sächsischen Gesellschaft der Wissenschaften 32 (6), 1–89.

Xomeritakis, G., Lin, Y.S., 1994. Chemical vapor deposition of solid oxides in porous media for ceramic membrane preparation. Comparison of experimental results with semianalytical solutions. Ind. Eng. Chem. Res. 33 (11), 2607–2617.

Xu, Y.D., Yan, X.T., 2012. Chemical vapor infiltration. In: Chemical Vapor Deposition—An Integrated Engineering Design Approach for Advanced Materials. Springer, London, pp. 165–213.

Yoshikawa, N., Evans, J.W., 2002. Modeling of chemical vapor infiltration rate considering a pore size distribution. J. Am. Ceram. Soc. 85 (6), 1485–1491.

Zhang, W., Hüttinger, K.J., 2001. Chemical vapor infiltration of carbon—revised. Part I: model simulations. Carbon 39 (7), 1013–1022.

Zhang, W.G., Hüttinger, K.J., 2002. Simulation studies on chemical vapor infiltration of carbon. Compos. Sci. Technol. 62 (15), 1947–1955.

Zhu, Y.C., Schnack, E., 2013. Numerical modeling chemical vapor infiltration of SiC composites. J. Chem. Article Id 836187.

Zhu, Y.C., Schnack, E., Li, A.J., 2011. Multiphase field modeling chemical vapor infiltration of SiC/SiC composite. Proc. Appl. Math. Mech. 11 (1), 453–454.

Zhu, Y., Schnack, E., Rahman, A.M., 2013. Computer modeling chemical vapor infiltration of SiC composites. Comput. Mod. Eng. Sci. 92 (3), 315–326.

Ziegler-Devin, I., Fournet, R., Marquaire, P.M., 2007. Pyrolysis of propane for CVI of pyrocarbon. Part III: experimental and modeling study of the formation of pyrocarbon. J. Anal. Appl. Pyrol. 79 (1), 268–277.

Ziegler, I., Fournet, R., Marquaire, P.M., 2005a. Pyrolysis of propane for CVI of pyrocarbon. Part I: experimental and modeling study of the formation of toluene and aliphatic species. J. Anal. Appl. Pyrol. 73 (2), 212–230.

Ziegler, I., Fournet, R., Marquaire, P.M., 2005b. Pyrolysis of propane for CVI of pyrocarbon. Part II: experimental and modeling study of polyaromatic species. J. Anal. Appl. Pyrol. 73 (2), 231–247.

Ziegler, I., Fournet, R., Marquaire, P.M., 2005c. Influence of surface on chemical kinetics of pyrocarbon deposition obtained by propane pyrolysis. J. Anal. Appl. Pyrol. 73 (1), 107–115.